The Pacific decadal oscillation, revisited

Matthew Newman[1,2*], Michael A. Alexander[2], Toby R. Ault[3], Kim M. Cobb[4], Clara Deser[5], Emanuele Di Lorenzo[4], Nathan J. Mantua[6], Arthur J. Miller[7], Shoshiro Minobe[8], Hisashi Nakamura[9], Niklas Schneider[10], Daniel J. Vimont[11], Adam S. Phillips[5], James D. Scott[1,2], and Catherine A. Smith[1,2]

[1]CIRES, University of Colorado, Boulder, Colorado
[2]NOAA Earth Systems Research Laboratory, Boulder, Colorado
[3]Department of Earth and Atmospheric Sciences, Cornell University, Ithaca, New York
[4]School of Earth and Atmospheric Sciences, Georgia Tech, Atlanta, Georgia
[5]Climate and Global Dynamics, National Center for Atmospheric Research, Boulder, Colorado
[6]NOAA Southwest Fisheries Science Center, Santa Cruz, California
[7]Scripps Institution of Oceanography, La Jolla, California
[8]Graduate School of Science, Hokkaido University, Sapporo, Japan
[9]Research Center for Advanced Science and Technology, The University of Tokyo, Tokyo, and Application Laboratory, JAMSTEC, Yokohama, Japan
[10]Department of Oceanography and International Pacific Research Center, University of Hawai`i at Manoa, Honolulu, Hawaii
[11]Department of Atmospheric and Oceanic Sciences, and Nelson Institute Center for Climatic Research, University of Wisconsin-Madison, Madison, Wisconsin

Submitted to *J. Climate*, October 28 2015
Revision submitted to *J. Climate*, February 19 2016
Accepted, March 1 2016

[*] *Corresponding author address:* Matthew Newman, NOAA/ESRL, 325 Broadway, R/PSD1, Boulder, CO 80305.
E-mail: matt.newman@noaa.gov

Abstract

The Pacific decadal oscillation (PDO), the dominant year-round pattern of monthly North Pacific sea surface temperature (SST) variability, is an important target of ongoing research within the meteorological and climate dynamics communities, and is central to the work of many geologists, ecologists, natural resource managers, and social scientists. Research over the last fifteen years has led to an emerging consensus: the PDO is not a single phenomenon, but is instead the result of a combination of different physical processes, including both remote tropical forcing and local North Pacific atmosphere/ocean interactions, which operate on different timescales to drive similar PDO-like SST anomaly patterns. How these processes combine to generate observed PDO evolution, including apparent regime shifts, is shown using simple autoregressive models of increasing spatial complexity. Simulations of recent climate in coupled GCMs are able to capture many aspects of the PDO, but do so based on a balance of processes often more independent of the Tropics than is observed. Finally, it is suggested that assessment of PDO-related regional climate impacts, reconstruction of PDO-related variability into the past with proxy records, and diagnosis of Pacific variability within coupled GCMs should all account for the effects of these different processes, which only partly represent direct forcing of the atmosphere by North Pacific Ocean SSTs.

1. Introduction

Since its identification in the late 1990's as the dominant year-round pattern of monthly North Pacific sea surface temperature (SST) variability, the Pacific decadal oscillation (PDO) has been connected both to other parts of the climate system and to impacts on natural resources and marine and terrestrial ecosystems. Subsequent research, however, has found that the PDO is not a single physical mode of climate variability but instead largely represents the combination of three groups of processes: (1) changes in ocean surface heat fluxes and Ekman (wind-driven) transport related to the Aleutian low, due to both local unpredictable weather noise and to remote forcing from interannual to decadal tropical variability (largely El Niño) via the "atmospheric bridge"; (2) ocean memory, or processes determining oceanic thermal inertia including "re-emergence", that act to integrate this forcing and thus generate added PDO variability on interannual and decadal time scales; and (3) decadal changes in the Kuroshio-Oyashio current system, forced by winds over the North Pacific driving westward propagating oceanic Rossby waves, manifested as SST anomalies along the subarctic front at about 40ºN in the western Pacific ocean. Thus, the PDO represents the effects of different processes operating on different timescales, and its apparent impacts elsewhere only partly represent direct forcing of the atmosphere by the North Pacific Ocean. What has often been characterized as PDO impacts in the literature may, in fact, reflect correlations with processes that drive simultaneous variations in *both* the PDO and the impact variables. Consequently, care should be taken when positing the PDO as a forcing of non-oceanic responses without a convincing argument for the physical forcing mechanism.

This paper synthesizes this current view of the PDO and discusses its implications for climate diagnosis, including PDO climate impacts and predictability (both oceanographic and atmospheric); potential decadal regime-like behavior; PDO simulations in climate models; the interpretation of multicentennial PDO reconstructions; and its relationship to another widely used index, the Interdecadal Pacific Oscillation (IPO). We conclude with a few suggested best practices for future PDO-based diagnosis and forecasts.

2. What is the PDO?

The PDO was first introduced by Mantua et al. (1997) as the leading Empirical Orthogonal Function (EOF) of North Pacific (20º-70ºN) SST monthly-averaged anomalies, or SSTAs, defined as departures from the climatological annual cycle *after removing the global mean SSTs*. Figure 1a shows the PDO pattern, calculated by regressing SST anomalies on the associated Principal Component (PC) time series, obtained from the HadISST dataset (Rayner et al. 2003) for the years 1901-2014. [Unless otherwise noted, this SSTA dataset and period are used for all calculations in this paper.] Over this period, the PDO is fairly similar across four SST datasets, all using different methods to fill in missing grids, with relatively minor differences both in time series (Fig. 1b) and pattern. The latter point can be illustrated using the Taylor diagram (Taylor et al. 2001) in Fig. 2, which shows that the root-mean-square (rms) differences between the HadISST PDO pattern and PDO patterns determined from the other SST datasets are relatively small. The PDO is also reasonably robust to sampling; for example, continually repeating the EOF analysis upon randomly chosen (with replacement) 50-year draws from the HadISST dataset yields patterns all highly similar to the PDO EOF (as shown by the black dots in Fig. 2). Dataset dependencies are more pronounced early in the

observational record, especially prior to about 1920 (Fig. 1b, bottom panel) or when only a few decades are used to define the climatology and leading EOF (Wen et al. 2014).

Initial research in the 1990's suggested that the PDO might represent a distinct physical "mode" of North Pacific variability. First, even using monthly anomalies, the PDO time series has a slowly varying component, with episodic changes of sign; hence "decadal oscillation"[1]. Second, low *simultaneous* correlation between time series of the PDO and eastern equatorial Pacific SST anomalies made the PDO and the Tropics appear only weakly coupled. Additionally, some early modeling work (Latif and Barnett 1994; 1996) raised the possibility that the PDO might correspond to a physical mode, oscillating on decadal time scales, of coupled atmosphere-ocean interaction within the North Pacific.

As the leading North Pacific EOF, the PDO is, by construction, the single pattern that best encapsulates variability of monthly SSTAs within the domain where it is defined. However, the PDO is also associated with variability outside the North Pacific, and indeed the observed regression pattern in Fig. 1a shows a strong connection between the North Pacific and the Tropics, despite relatively low correlation values within the narrow cold tongue located in the eastern equatorial Pacific between 2ºN-2ºS (not shown; see Deser et al. 2004). In particular, positive SSTAs in the eastern tropical Pacific accompany negative SSTAs in the central and western North Pacific and positive SSTAs in the eastern North Pacific (Fig. 1a). Some PDO details depend on the domain used for the EOF calculation: as this domain is expanded southward (orange symbols in Fig. 2),

[1] Note that in meteorological parlance, "oscillation" was first related to *spatial* sea-saw patterns in the Atlantic and Pacific by Walker and Bliss (1932), but has more recently been occasionally confused with *temporal* oscillations.

the tropical portion of the pattern becomes relatively more pronounced, even along the equator, with the North Pacific anomaly shifting slightly eastward to become more symmetric with its South Pacific counterpart. The leading SST EOF of the entire Pacific basin resembles a global ENSO-related pattern (e.g., Deser and Blackmon 1995).

While the PDO exists throughout the year, it undergoes some seasonal evolution both in amplitude and structure. The PDO's amplitude is greatest from November through June, with weak maxima both in mid-winter and late spring and a pronounced late summer/early fall minimum (Wang et al. 2012). However, repeating the PDO regression separately by month shows the SSTA maximum shifting from the northeastern to northwestern Pacific between the cold and warm seasons (not shown). In fact, the largest PDO-related SSTAs in the northwestern Pacific occur in early fall despite the overall PDO minimum then. In the observed PDO autocorrelation structure (Fig. 1c), for long lags persistence is increased (decreased) in spring (autumn) (i.e., the tilted ridges/troughs at long leads/lags in Fig. 1c).

3. Processes driving the PDO

Statistical modes may represent physical modes, but there need not be a one-to-one correspondence between them. A body of research exists showing how different physical processes, including random atmospheric forcing; teleconnections from the tropical Pacific; and ocean Rossby waves/shifts in the basin-wide ocean gyre circulation, contribute to PDO variability on a variety of time scales and regions in the North Pacific Ocean.

3.1 FLUCTUATIONS IN THE ALEUTIAN LOW (LARGE-SCALE STOCHASTIC FORCING)

Many aspects of climate can be represented by a slow dynamical system integrating fast forcing approximated as random, or stochastic, noise (Hasselmann 1976). In a simple stochastic model of midlatitude SST variability (Frankignoul and Hasselmann 1977), the ocean at a given location is treated as a motionless (well-) mixed layer in which surface heat fluxes both force and damp SSTAs. The forcing F is represented by fluxes associated with weather variations, which relative to oceanic time scales have approximately no memory and the same variance at all time scales (effectively, white noise). The resulting SSTAs are damped by a linear negative air-sea feedback, representing loss (gain) of heat with the atmosphere from anomalously warm (cold) waters. This can be expressed as a first order autoregressive or *AR1* model,

$$SSTA(n) = r\, SSTA(n\text{-}1) + F, \quad (1)$$

where r represents the expected fraction of the SSTA retained between times n-1 and n, determined by the feedback of air-sea heat fluxes and SST and by the thermal inertia of the upper ocean in direct contact with the atmosphere. Then the SSTAs exhibit a red noise spectrum whose magnitude increases with the inverse square of frequency, flattening out at periods long compared to the damping time scale.

The simple view of SST variability as the result of noise integration can be applied basin-wide. White noise forcing associated with large-scale weather patterns generates much of the observed SST variability over the entire North Pacific Ocean (Frankignoul and Reynolds 1983), where interannual variability in the surface fluxes and SSTs are closely linked to dominant atmospheric circulation patterns (Cayan 1992;

Iwasaka and Wallace 1995). For example, in an atmospheric general circulation model (AGCM) coupled to a mixed layer ocean model with no currents (and hence no ENSO variability or ocean dynamics), the dominant sea level pressure (SLP) pattern is associated with fluctuations in the strength of the Aleutian low pressure system primarily resulting from internal atmospheric dynamics (Pierce 2001; Alexander 2010), including large-scale dominant atmospheric teleconnection patterns such as the Pacific-North American (PNA) pattern. For periods with a stronger Aleutian low, enhanced wind speeds and reduced air temperature and humidity along ~35°N cool the underlying ocean via surface sensible and latent heat fluxes, while northward advection of warm moist air heats the ocean near North America (cf. Fig. 1a); the opposite flux anomalies occur when the low is weaker than average. This simulated flux-driven SSTA pattern in the North Pacific closely resembles the observed PDO. Anomalous Ekman transports tend to amplify the flux-driven pattern (Miller et al. 1994b; Alexander and Scott 2008).

These physical processes result in observed correlations in which atmospheric variations generally lead SST variations (eg, Davis 1976; Deser and Timlin 1998). For example, Fig. 3a shows the PDO-like pattern that results from springtime SST correlation with prior wintertime Aleutian low variability (here measured by the North Pacific index (NPI); Trenberth and Hurrell 1996). Throughout the cold season, Aleutian low variability typically leads the PDO, even over consecutive years (Fig. 3b). Note that the NPI and PDO are also simultaneously correlated, which has been misinterpreted as indicating that the PDO must force an Aleutian low response. As Frankignoul (1999) noted, even without oceanic feedback onto the atmosphere, simultaneous extratropical atmosphere-SST correlation can occur due to rapid weather forcing of the more slowly evolving

ocean; so, to diagnose interactions between the North Pacific Ocean and the Aleutian low requires determining both positive and negative PDO-NPI lag correlations.

3.2 TELECONNECTIONS FROM THE TROPICS

a. The atmospheric bridge

We now generalize the "PDO-as-integrator" paradigm in (1), allowing for other sources of forcing F beyond noise due to intrinsic mid-latitude atmospheric variability. ENSO tropical Pacific SSTAs induce tropical precipitation shifts forcing global atmospheric teleconnections (e.g., Trenberth et al. 1998; Liu and Alexander 2007), altering near-surface air temperature, humidity, wind, and clouds far from the equatorial Pacific. The resulting variations in the surface heat, momentum, and freshwater fluxes cause changes in SST and ocean currents. Thus, during ENSO events an "atmospheric bridge" extends from the equatorial Pacific to other ocean basins including the North Pacific (e.g., Alexander 1990, 1992; Lau and Nath 1994, 1996, 2001; Alexander et al. 2002). When El Niño events peak in boreal winter, the Aleutian low deepens and the changes in the surface heat fluxes, wind driven mixing, and Ekman transport in the upper ocean all act to create a positive PDO SSTA pattern (Alexander et al. 2002, Alexander and Scott 2008; see also Strong and Magnusdottir 2009).

The atmospheric bridge is seen when correlating a wintertime ENSO index (here, defined as the time series of the leading tropical SSTA EOF determined within the 18ºS-18ºN domain) with subsequent global springtime SSTAs (Fig. 3c). This correlation pattern is stable throughout the observational record, with some amplitude changes but relatively little modification in pattern (not shown). In general, ENSO leads the PDO throughout the year (Fig. 3d), but the bridge acts differently in summer and fall compared

207 to winter, modifying SSTAs in the west Pacific primarily through changes in cloudiness
208 (Alexander et al. 2004).

209 *b. Oceanic coastally trapped waves*

210 The equatorial thermocline variability associated with ENSO excites Kelvin and
211 other coastally trapped ocean waves that propagate poleward along the eastern Pacific
212 boundary in both hemispheres, generating substantial sea level and SST anomalies
213 (Enfield and Allen 1980; Chelton and Davis 1982; Clarke and van Gorder 1994).
214 However, these waves impact the ocean only within ~50 km of shore poleward of 15°N
215 (Gill 1982).

216 *c. Tropical decadal variability*

217 Tropical Pacific decadal variations will also be communicated to the North
218 Pacific via the atmospheric bridge, driving about ¼ - ½ of the PDO-related variability
219 based on GCM model experiments (Alexander et al. 2002; Alexander 2010). Zhang et al.
220 (1997) employed several techniques to separate observed interannual and "interdecadal"
221 (> 6 yr) ENSO variability. The SSTA pattern based on their low-pass filtered data is
222 similar to the unfiltered ENSO pattern, except meridionally broader in the eastern
223 equatorial Pacific and higher amplitude both in the central equatorial Pacific and in the
224 extratropics; its North Pacific component resembles the PDO. Other statistical methods
225 have found similar structures and have indicated that some PDO decadal variability is
226 associated with low frequency anomalies in the tropical Pacific (e.g. Nakamura et al.
227 1997; Power et al. 1999; Mestas Nuñez and Enfield 1999; Barlow et al. 2001; Seager et

al. 2004; Deser et al. 2004; Vimont 2005; Alexander et al. 2008a; Chen and Wallace 2015).

How much tropical Pacific decadal variability is due to coupled processes operating on fundamentally decadal time scales, including possible linkages to the North Pacific (see section 3.3d, below), and how much is the residual of weather noise-driven ENSO dynamics (eg, Newman et al. 2011; Wittenberg et al. 2014), remains to be determined. Because the decadal ENSO pattern is similar to the most persistent portions of the seasonally evolving ENSO pattern, it may be partly the residual of a non-uniformly evolving interannual phenomenon (Vimont 2005) and/or the asymmetry between warm and cold phases of ENSO (Rodgers et al. 2004).

3.3 MIDLATITUDE OCEAN DYNAMICS AND COUPLED VARIABILITY

a. Re-emergence

We might expect that, due to the thermal capacity of seawater and typical mixed layer depths, the memory time scale of the upper ocean is on the order of months. However, due to seasonal variations in the oceanic mixed layer depth, the decorrelation time scale of midlatitude SSTAs in successive cold seasons is generally greater than a year. Figure 4a-c illustrates this process, showing the correlation of FMA PDO values with ECMWF ORAS4 (Balmaseda et al. 2013) ocean temperatures at depth and increasing lag for three regions of the North Pacific. Similar results are obtained using the SODA dataset (Carton and Giese 2008; not shown) and in modeling studies (eg, Alexander et al. 2002; Wang et al. 2012). Persistent temperature anomalies forming at the surface mix downwards throughout the deep winter mixed layer. Then, when the mixed

250 layer abruptly shallows in spring, thermal anomalies at depth can remain under the
251 summer seasonal thermocline, insulated from surface fluxes that damp anomalies in the
252 thin mixed layer above. When the mixed layer deepens again in the following fall, the
253 deeper anomalies are mixed back towards the sea surface. This process, first noted by
254 Namias and Born (1970, 1974) and termed the "reemergence mechanism" by Alexander
255 and Deser (1995), occurs over large portions of the North Atlantic and North Pacific
256 Oceans (Alexander et al. 1999; 2001; Bhatt et al. 1998; Timlin et al. 2002; Hanawa and
257 Sugimoto 2004). The PDO SSTA pattern, generated by internal atmospheric dynamics
258 and/or the atmospheric bridge, recurs in consecutive winters via the reemergence
259 mechanism (Alexander et al. 1999, 2001, 2002), while the summertime PDO signal (at
260 the surface, at least) does not tend to recur (Nakamura and Yamagata 1999) and is instead
261 largely forced by contemporaneous air-sea fluxes. The effects of reemergence can extend
262 into a second year, as evidenced in Fig. 4 by the cold season maxima in both years 1 and
263 2.

264 Thus, the reemergence mechanism determines the effective thermal inertia and
265 the value of r in (1) as corresponding to deep winter mixed layers (Deser et al. 2003),
266 enhancing PDO variability on interannual to decadal time scales (Newman et al. 2003;
267 Schneider and Cornuelle 2005). The impact of reemergence is evident in the observed
268 PDO lag autocorrelation structure (Fig. 1c). For example, while year-to-year PDO
269 autocorrelation is over 0.45 in late winter and spring, it drops below 0.3 in late summer
270 and autumn. Also, the PDO is significantly correlated over three consecutive springs but
271 is nearly uncorrelated over three consecutive autumns.

b. Ocean gyre dynamics

Much of the large-scale dynamics within the North Pacific Ocean involves two basin-wide circulations of water, a counterclockwise subpolar gyre and clockwise subtropical gyre, separated by a sharp meridional SST gradient called the subarctic frontal zone (SAFZ). In the western Pacific, large SST variations associated with the PDO occur within the SAFZ, specifically in the Kuroshio Extension (KE) and Oyashio frontal zones and the mixed water region in between (Nakamura et al. 1997; Nakamura and Kazmin 2003; Nonaka et al. 2006; see, for example, Fig. 5 in Frankignoul et al. 2011). While in most of the North Pacific, SST variability is driven primarily by atmospheric forcing (Smirnov et al. 2014), in this region persistent warm (cool) SSTAs in winter tend to enhance (reduce) heat and moisture fluxes into the atmosphere (Tanimoto et al. 2003; Taguchi et al. 2012), a consequence of dynamic adjustment of upper-ocean gyre circulations that contributes to F in (1). The adjustment occurs primarily through westward propagating Rossby waves excited by anomalous wind stress curl (Miller et al. 1998; Deser et al. 1999; Seager et al. 2001; Schneider et al. 2002; Qiu and Chen 2005; Taguchi et al. 2007). These waves, whose sea surface height variations can be measured by satellite (Fig. 5b), take ~3-10 years to cross the basin guided by the KE jet (Sasaki and Schneider 2011; Sasaki et al. 2013), producing primarily decadal variability in F with a red spectra without preferred spectral peaks (Frankignoul et al. 1997). Specifically, SSTAs result (Fig. 5a) from shifts of latitude and intensity of the fronts (Qiu 2003; Nakamura and Kazmin 2003; Taguchi et al. 2007), and modulations of the stability of the KE jet, the recirculation gyre (Qiu 2000, 2002; Qiu and Chen 2005, 2010; Kelly et al. 2010; Kwon et al. 2010) and thereby oceanic eddy-driven heat transports (Sugimoto

295 and Hanawa 2011). The latitude of the shallow Oyashio front, by contrast, may be more
296 sensitive to local wind forcing (Nonaka et al. 2006; 2008). Decadal SSTAs in the KE and
297 Oyashio regions have undergone long-term amplitude modulations, suggesting that this
298 contribution from extratropical air-sea interaction to the PDO may vary on multi-decadal
299 scales (Miyasaka et al. 2014).

300 An atmospheric response to PDO SST variations could enhance PDO decadal
301 variance, or lead to a preferred time scale, if the response projects on F in (1) as a
302 positive or delayed negative, respectively, feedback on the PDO. A basic thermodynamic
303 response exists: the temperature difference between atmospheric boundary layer and
304 oceanic mixed layer decreases due to air-sea heat exchange, slowing subsequent heat
305 exchanges that depend upon this difference, producing "reduced thermal damping"
306 (Barsugli and Battisti 1998) and related increase of temperature variability (Bladé 1997).
307 Stochastic wind forcing whose spatial scale corresponds to certain ocean advective scales
308 might also resonantly enhance decadal SST variability without other feedbacks
309 (Saravanan and McWilliams 1998).

310 The coupled ocean-atmosphere dynamical response to PDO SSTAs has been less
311 clear. Latif and Barnett (1994, 1996) suggested that west Pacific SST anomalies resulting
312 from Aleutian low-forced Rossby wave adjustment of the subtropical gyre (described
313 above) drive an atmospheric response that, via the wind stress curl, reverses the sign of
314 the subtropical gyre anomaly and the corresponding central North Pacific SST anomaly.
315 This negative feedback in the west Pacific initiates the opposite phase of a 20-yr PDO
316 oscillation. However, the necessary west Pacific atmospheric response appears to be of
317 the wrong sign to generate sustained oscillations (Schneider et al 2002). In particular,

318 when the Aleutian Low strengthens, it also shifts southward; as a result, the gyre
319 circulation shifts equatorward, and the SST anomalies subsequently cool rather than
320 warm in the KE region (Deser et al., 1999; Miller and Schneider 2000; Seager et al.
321 2001). In addition, surface heat fluxes damp SST anomalies in the KE region both in
322 observations and ocean model hindcasts (Seager et al., 2001; Schneider et al. 2002;
323 Tanimoto et al., 2003; Kelly, 2004). Note also that the length of the Latif and Barnett
324 model run was relatively short – their result was not reproduced in a longer run of the
325 model (Schneider et al 2002) – whereas large model ensembles are now used to discern
326 SSTA-forced signals from undersampled atmospheric noise (eg, Sardeshmukh et al 2000;
327 Deser et al. 2004).

328 Still, recent observational studies (Frankignoul et al. 2011; Taguchi et al. 2012),
329 coupled model experiments (Wu et al. 2003; Kwon and Deser 2007; Taguchi et al. 2012)
330 and observationally derived heuristic models (Qiu et al. 2007) suggest that the
331 atmospheric response to SSTAs in the KE and Oyashio frontal zones could induce a
332 modest atmospheric response in the anomalous Aleutian low, which may be able to
333 enhance variability at decadal periods. Those SST frontal zones may act to anchor the
334 Pacific storm track (Nakamura et al. 2004), and its feedback forcing from synoptic-scale
335 eddies migrating along the storm track seems important in maintaining a stationary
336 atmospheric response (Taguchi et al. 2012; Okajima et al. 2014). However, AGCM
337 studies continue to disagree on even the sign of the atmospheric response to frontal zone
338 SSTAs, with sensitivity to many factors including the simulated direct response to the
339 low-level heating, downstream eddy feedbacks of the modulated storm track, and
340 dependencies upon seasonality and base state (Okajima et al. 2014; see also review by

Kushnir et al. 2002). Also, Frankignoul et al. (2011) and Taguchi et al. (2012) observed an anomalous surface Aleutian Low in response to KE/Oyashio fronts SSTAs that, however, was accompanied by different upper-level anomalies. Some recent observational analysis, and model experiments at finer resolution (typically ~25 km), suggests that a robust atmospheric response to KOE SSTAs may involve significant changes in poleward heat and moisture transports by individual storms (O'Reilly and Czaja 2014) that are not well captured by currently typical (~1º) climate model atmospheric resolution (Smirnov et al. 2015), so the impact of ocean-atmosphere coupling onto the PDO remains not well understood.

c. Summertime air-sea feedbacks

During summer, due to both a shallower seasonal thermocline and weaker atmospheric variability, the PDO tends to be less persistent and less confined to the oceanic frontal zones (Nakamura and Kazmin 2003), although the spatial structure of the PDO is not fundamentally changed (Chen and Wallace 2015). Instead, SST variability may be linked to anomalous low-level cloudiness. Over the NE Pacific, for example, where summertime mid-tropospheric subsidence is maintained by the climatological subtropical high (Miyasaka and Nakamura 2005), most of the clouds develop under the capped inversion layer (Klein et al. 1995: Norris 1998; Wood 2012). Decadal enhancement of lower-tropospheric static stability, due both to cooler SSTAs and stronger subsidence associated with the intensified subtropical high, acts to increase low-level cloud amount, optical depth and planetary albedo, and vice versa (cf. Clement et al. 2009). The resulting anomalous cloud radiative forcing could enhance the underlying SSTA as positive feedback. Over the NW Pacific, low-level cloudiness is

364 climatologically high in summer, but is less variable than over the NE Pacific (Norris et
365 al. 1998), which is particularly the case over the subpolar oceanic gyre. Still, decadal
366 variability in low-level cloudiness tends to maximize around 35°N to the south of the NP
367 SAFZ. Schwartz et al. (2014) show that the summertime coastal low clouds all along the
368 West Coast vary in concert with PDO-related SST variations.

369 *d. North Pacific impacts on tropical variability*

370 While the atmospheric bridge primarily extends from the tropics to the
371 extratropics, North Pacific SSTA variability may also influence the tropical Pacific. In
372 the "seasonal footprinting mechanism" (Vimont et al. 2001, 2004), wintertime weather
373 noise alters surface heat fluxes to create SST anomalies that in the subtropics persist
374 through summer. These SST anomalies, which are largely orthogonal to the PDO since
375 they instead reflect the second EOF of North Pacific SSTAs (Bond et al. 2003),
376 associated with the North Pacific Gyre Oscillation (NPGO; Di Lorenzo et al 2008), drive
377 near-equatorial zonal wind stress anomalies impacting ENSO variability (Vimont et al.
378 2003, 2009; Alexander et al. 2008, 2010; Di Lorenzo et al. 2010; Wang et al. 2012). On
379 longer time scales, in some models the atmospheric response to slowly varying KE SST
380 anomalies extends deep into the Tropics to affect decadal ENSO variability (Barnett et al.
381 1999; Kwon et al. 2010).

382 A coupled extratropical-tropical mechanism for decadal variability proposed by
383 Gu and Philander (1997) involves subduction of North Pacific mixed layer temperature
384 anomalies from the surface layer into the thermocline and their subsequent southward
385 advection by the subtropical cell (STC) to upwell at the equator. However, observational
386 analyses showed that subducted central North Pacific anomalies decay prior to reaching

387 the Tropics (Deser et al. 1996; Schneider et al. 1999; Capotondi et al. 2003; Sasaki et al.
388 2010; Li et al. 2012). Alternatively, variations in subtropical winds (which may also be
389 noise driven) alter the strength of the STC overturning circulation, changing its
390 southward advection of relatively cold extratropical water that, upwelling at the equator,
391 drives tropical air-sea feedbacks and hence decadal variability. This mechanism, evident
392 in some models (Kleeman et al. 1999) although possibly confined to within about 20º of
393 the equator (Capotondi et al. 2005), is supported by observational analyses (McPhaden
394 and Zhang 2002; Zhang and McPhaden 2006). Note that even if this mechanism does not
395 extend into the North Pacific it still impacts the PDO by modifying its tropical forcing.

396 **4. The PDO as the sum of multiple processes**

397 In this section we employ two approaches, empirical and numerical modeling studies, to
398 explore how PDO processes combine to produce PDO variability and dynamics and,
399 potentially, PDO regime shifts.

400 4.1 EMPIRICAL AUTOREGRESSIVE MODELS

401 Several recent studies extended the simple AR1 model (1) to incorporate additional PDO
402 dynamical processes discussed above. Using annually-averaged (July-June) anomalies,
403 Newman et al. (2003) found that (1) could be improved by including ENSO forcing
404 within *F*, extending the AR1 model to

405 $$PDO(n) = r\, PDO(n\text{-}1) + a\, ENSO(n) + noise\ . \qquad (2)$$

406 Note that *r*, which corresponded to a time scale of about two years, included
407 reemergence, amplifying the low-frequency ENSO component of PDO variability to
408 produce a “reddened ENSO”. Schneider and Cornuelle (2005) included both shifts in the

North Pacific Ocean gyres and explicit representation of anomalous Aleutian low forcing in *F* to show that on interannual time scales, random Aleutian Low fluctuations and ENSO teleconnections were about equally important in determining PDO variability with negligible contributions from ocean currents, while on decadal time scales stochastic forcing, ENSO, and changes in the gyre circulations each contributed approximately 1/3 of the PDO variance. The primary implication of these analyses is that, unlike ENSO, the PDO is likely not a single phenomenon but rather the sum of several different basin-scale processes (eg; Schneider and Cornuelle 2005; Newman 2007, 2013; Alexander et al. 2008b).

As (1) is extended into (2) by including observed, non-stochastic forcing in *F*, it is no longer strictly speaking an AR1 model, nor is it a closed model. Also, while the patterns corresponding to these processes are not identical and their characteristic time scales are quite different, they all project strongly onto the PDO pattern. However, many common multivariate analysis techniques cannot distinguish between spatially similar, or nonorthogonal, patterns with differing evolution.

These problems can be addressed by extending the AR1 model to many variables,

$$\mathbf{x}(n) = \mathbf{G}\,\mathbf{x}(n-1) + \boldsymbol{\eta}_s, \qquad (3)$$

where $\mathbf{x}$ is now a multivariate state vector and $\boldsymbol{\eta}_s$ represents noise. In the following, $\mathbf{x}$ represents maps of SSTAs covering the tropical (18ºS-18ºN) and North Pacific (20ºN-70ºN) oceans. The resulting multivariate AR1 model (Linear Inverse Model (LIM); Penland and Sardeshmukh 1995; Newman 2007; Alexander et al. 2008b) yields patterns representing different dynamical processes with different evolutions, which are independent but not orthogonal -- that is, they have potentially similar spatial structure. In

analogy with (1), each pattern (each eigenmode of **G**) is associated with a time series that has its own value of *r* (the real part of its eigenvalue), but not all the patterns are static (some also propagate with characteristic frequency given nonzero imaginary eigenvalue). Here we extend the Newman (2007) LIM to finer spatial (2ºx2º) and temporal (3-month running mean) resolution (details of the approach, including strengths and weaknesses, can be found there and the many papers cited therein); similar to that study and related LIM analyses (Compo and Sardeshmukh 2010; Newman 2013), the leading eigenmode's pattern (not shown) is the departure of the local SST trend from the global mean SST trend and makes almost no contribution to the PDO. Results below are also little changed using a linearly-detrended dataset (Newman 2013).

Ordered by decreasing *r*, the three eigenmodes in Fig. 6 represent dynamical processes with maxima in the North, central tropical/northern subtropical, and eastern tropical Pacific, respectively; similar patterns from various analyses have been reported elsewhere (eg, Barlow et al. 2001; Chiang and Vimont 2004; Guan and Nigam 2008; Compo and Sardeshmukh 2010). The first eigenmode represents largely North Pacific dynamics. The latter two represent interannual to decadal tropical dynamics driving North Pacific variability (Newman 2007), consistent with Schneider and Cornuelle (2005); their tropical portions form a simple basis for ENSO evolution including its "flavors" or diversity (e.g., Penland and Sardeshmukh 1995; Trenberth and Stepaniak 2001; Takahashi et al. 2011; Capotondi et al. 2015). Each eigenmode's projection on the PDO EOF yields time series (also in Fig. 6) that when summed result in a "reconstructed" PDO (Fig. 6g) quite similar to the full PDO (Fig. 6h), with 0.7 correlation that increases to over 0.8 when both are smoothed with the 6-yr lowpass filter used in Fig. 1b. The

455 residual between the two time series, representing the contributions of other eigenmodes
456 (not shown), is likely primarily noise since its decorrelation time scale is ~5 months.
457 The PDO appears to undergo rapid transitions between extended periods of
458 opposite phase every few decades or so (e.g., Ebbesmeyer et al. 1991; Graham 1994;
459 Mantua et al. 1997; Minobe 1997; Fleming 2009; Minobe 2012), as denoted by the green
460 lines in Fig. 6h. Such "regime shifts" (if significant; see Rudnick and Davis 2003) might
461 represent sudden nonlinear changes between relatively stable climate states. However,
462 similar behavior is also well known to exist in aggregations of AR1 processes (Granger
463 1980; Beran 1994); that is, in (3). So, to the extent that the PDO represents an
464 aggregation of several basin-scale dynamical processes with differing, but substantial,
465 projection onto the PDO pattern, each PDO regime could result from different
466 combinations of processes (see also Deser et al. 2004), with apparent regime shifts due to
467 randomly forced variations in the superposition of these processes (Newman 2007) as
468 captured by the reconstructed PDO in Fig. 6g. In other words, PDO climate regime shifts
469 could be partly an artifact of measuring the multivariate North Pacific Ocean climate
470 system with a single index.
471 As a corollary, a PDO regime shift need not correspond to pronounced changes
472 throughout the North Pacific. This point is illustrated by comparing multidecadal SST
473 change across 1976/77 relative to change across 1969/70. The latter time is not typically
474 identified with a Pacific regime shift (although see Baines and Folland 2007), but it is
475 when the time series of the most slowly varying PDO component ended a long period of
476 negative values (Fig. 6a). For the 1976/77 regime shift between 20-year epochs (Fig. 7b),
477 the well-documented warming in the Tropical IndoPacific and along the west coast of

North America is evident, along with central Northeast Pacific cooling (e.g., Graham 1994; Miller et al. 1994a; Meehl et al. 2009). However, North Pacific multidecadal cooling across 1969/70 (Fig. 7a) was stronger and extended farther westward; note also a corresponding Atlantic signal. These two figures together show that the multidecadal shifts in tropical and North Pacific SSTs were not coincident but rather occurred some years apart, and may not have corresponded to a coherent basin-wide Pacific climate regime shift.

4.2 PDO REPRESENTATION BY COUPLED CLIMATE MODELS

Perhaps our most comprehensive tool for understanding how processes interact to produce the PDO is the coupled general circulation model (CGCM). Here, we assess CGCM reproduction of the PDO and PDO processes.

Figure 8 exemplifies the range of PDO patterns (defined according to Mantua et al. 1997) across the historical CMIP5 model runs, in comparison with the observed pattern (Fig. 1a). All CMIP5 PDO patterns are available at http://www2.cesm.ucar.edu/working-groups/cvcwg/cvdp (Phillips et al. 2014). Some models can depict the observed spatial pattern ("Model A") while others lack the tropical connection ("Model B"). Also shown are two PDO patterns, chosen to be closest ("A") and farthest ("B") from observations, generated from two ensemble members taken from the same CGCM, the Community Earth System Model Large Ensemble (CESM-LE; Kay et al. 2015). Here, the differences are entirely due to internally generated variability, since all other aspects of the experiment (including the model and external forcing) are fixed. We next use the Taylor diagram of Fig. 2 to quantify the degree of resemblance of the PDO pattern in each CMIP3, CMIP5 and CESM-LE model simulation with

observations (HadISST). Recall that the distance of each symbol from the reference (HadISST PDO) represents the rms difference of each model PDO pattern. The North Pacific SSTA pattern of each model ensemble member is broadly similar to observations, and is accompanied by a realistic SLP anomaly that is consistent with the atmosphere forcing the ocean and not vice versa (see also Sheffield et al. 2013; Yim et al. 2014), but Fig. 2 shows that the simulations are generally outside the range of observational dataset and sampling uncertainty. Comparing the CMIP5 and CESM-LE values in Fig. 2 suggests that PDO simulation uncertainty may be due more to differences between models than to differences between realizations. Some modest improvement of the PDO simulation from CMIP3 to CMIP5 is apparent (see also Polade et al. 2013), primarily through the reduction of outliers.

Due to the chaotic nature of the climate system, even very small differences in initial conditions cause simulations to diverge from one another and from nature. Hence, in the absence of an externally forced signal, we expect CGCMs to represent PDO variability statistics but not the observed PDO time series. Fig. 8c shows this expected range in CMIP5 historical PDO time series (smoothed with the 6-yr lowpass filter); in particular, none reproduce the observed 20th century sequence of PDO "regimes". Additionally, the ensemble mean of all the time series is near-zero. This is also the case for the CESM-LE ensemble mean, although the CMIP3 ensemble mean has a weak trend. Given that these model runs are forced with the post-1850 history of radiative forcing, Fig. 8c suggests that the externally forced PDO signal has been negligible, consistent with the empirical analysis in section 4.1, and that the PDO represents natural internal variability.

524 Figure 9 shows the lag autocorrelation of the PDO (Fig 9a), as well as the lagged
525 correlations between the PDO and the DJF Niño3.4 index (Fig. 9b) or DJF PNA index
526 (Fig. 9c), for each model ensemble member over its respective period, compared to
527 observations from 1901-2009. Most, but not all, simulated PDO time series are too
528 persistent. In all the models during winter, the PDO is too weakly correlated with both
529 the PNA and Niño3.4, yet many of the models then overestimate the lagged correlation
530 between these same indices and the PDO the following spring and summer, consistent
531 with too strong PDO persistence or with errors in the North Pacific seasonal cycle.
532 Previous analysis showed that almost all CMIP3 models underestimated the
533 ENSO-PDO relationship compared to observations (Newman 2007; Oshima and
534 Tanimoto 2009; Furtado et al. 2011; Lienert et al. 2011; Deser et al. 2012; Park et al.
535 2013). To investigate how the representation of tropical-extratropical interaction impacts
536 the PDO in the CMIP5 historical runs, we fit each PDO time series with the extended
537 AR-1 model

538 $$\mathrm{PDO}(n)=r\,\mathrm{PDO}(n\text{-}1) + a\,\mathrm{ENSO1}(n) + b\,\mathrm{ENSO2}(n) + \varepsilon(n), \quad (4)$$

539 where PDO is the PDO time series, ENSO1 and ENSO2 are the time coefficients of the
540 leading two EOFs of tropical Pacific (20°S–20°N) SSTAs, ε is white noise, and n is the
541 time step. This model, estimated for detrended and normalized annual mean time series
542 averaged from July to June, follows the approach introduced in (2) but includes potential
543 diversity in ENSO anomalies (Capotondi et al. 2015). ENSO1 and ENSO2 are
544 determined separately for each model and dataset and then annually averaged.
545 The extended AR-1 models constructed from observations and the CMIP5 runs
546 have several notable differences. First, tropical forcing of the PDO is dominated by

ENSO1 in observations, but not for most CMIP5 runs (Fig. 10b). Also, how well each extended AR-1 model represents each PDO time series is related to ENSO1 forcing strength: in Fig. 10, AR-1 model performance ρ, the correlation of each PDO time series with its corresponding estimate (4), and *a* are correlated at 0.7. On the other hand, CMIP5 ENSO2 forcing is generally greater than for observations (Fig. 10c). These results indicate that the tropics-to-PDO linkage in observations is different, both quantitatively and qualitatively, from most CMIP5 models, which may also be due to ENSO simulation errors (eg, Bellenger et al 2014; Capotondi et al. 2015). Also, note that most CMIP5 models overestimate *r* and underestimate the noise forcing, suggesting that mechanisms causing persistence of the PDO such as oceanic vertical mixing, SST reemergence, oceanic Rossby wave propagation, and/or ocean-to-atmosphere feedback in mid-latitudes play a stronger role in CMIP5 models than in observations. Why these errors exist remains to be understood, but together they suggest that most CGCM PDOs may be more independent of the Tropics than is observed.

5. Decadal-to-centennial PDO variability

As with simpler AR1 models, the LIM may be used to generate confidence intervals for power spectra, although unlike simpler AR1 models, LIM-generated variability can include broadband spectral peaks (such as ENSO; Newman et al. 2009; Ault et al. 2013). Figure 11 shows that PDO spectra calculated from all four observational data sets (black lines) and, for the most part, the CMIP5 simulations (both control and historical) all generally lie within the LIM confidence intervals, quantified using 140 different 1750-yr realizations of (3) (eg, Ault et al. 2013). So too do the 1000-yr, externally forced "last millennium" CMIP5 simulations that include estimates of explosive volcanism, solar

570 variability, and anthropogenic changes to atmospheric composition and land use since
571 850, again suggesting that the PDO largely represents internal, unforced variability, even
572 on decadal to centennial (or dec-cen) timescales. However, given that the CMIP5 PDO
573 connections to the Tropics are generally too weak and that unforced CMIP5 models
574 generally *underestimate* dec-cen tropical SST variability (Ault et al. 2013; Laepple and
575 Huybers 2014), the agreement between the CMIP5 power spectra and the LIM may be
576 somewhat fortuitous. That is, some "reddened ENSO" power in observations is missing
577 in the CMIP5 models, but its loss seems compensated by too-persistent internally-
578 generated North Pacific SSTAs.

579 Even relative to a univariate AR1 (red noise) process, no statistically significant
580 decadal or multidecadal peaks in these spectra are detectable (Pierce 2001). Rather, PDO
581 spectral power appears to continually increase with decreasing frequency f, raising the
582 possibility that the spectra represent not red noise but rather long-memory, "1/f noise"
583 (Keshner 1982), with potentially pronounced regime behavior (eg, Percival et al. 2001;
584 Overland et al. 2006; Fleming 2014; see also Fraedrich et al. 2004). However, note that
585 the LIM spectrum also is not flat over multidecadal time scales. In fact, spectral slopes
586 are characteristic not only of some nonlinear systems but also aggregations of processes
587 resulting from a multivariate AR1 system driven by noise (Milotti 1995; see also Penland
588 and Sardeshmukh 2012).

589 Spectra for several paleo-reconstructions of the PDO, made by combining proxies
590 such as tree rings, corals, and sediments (Table 1), stay below the upper LIM confidence
591 interval for decadal to multidecadal periods. Many of these reconstructions have been
592 used to suggest the existence of PDO multidecadal spectral peaks, particularly for periods

593 of about 20 and 70 years (eg, Biondi et al. 2001), although note that none of the
594 observational datasets show significant peaks on these time scales. However, poor
595 reproducibility between the various PDO reconstructions (Fig 11d) calls into question
596 their collective fidelity as paleo-PDO indices, even for the multi-decadal time scales that
597 multi-century record lengths should be able to resolve (Fig. 11e). Beyond profound
598 differences in the various proxy networks used to reconstruct the PDO, the
599 reconstructions also reflect differences in local climate variable responses to large-scale
600 atmospheric and oceanic variability, potential seasonal biases, and geographic domain
601 (e.g., Tingley, 2012; St. George, 2014). As most PDO reconstructions are based on tree
602 ring width timeseries, the statistical removal of biological growth-related trends in these
603 series (Cook et al., 1995; Jones et al., 2009 and references therein) may deflate
604 centennial-scale variability, removing spectral power at the lowest frequencies in Fig.
605 11c.

606 Because the PDO represents not one but many dynamical processes, it poses a
607 unique challenge as a target for proxy-based reconstruction. Thus far, reconstructions
608 have largely sought to reproduce and extend the PDO index itself. A more nuanced
609 approach that targets one or more of the different processes that contribute to PDO-
610 related variability would likely lead to an understanding about how such processes have
611 varied in the past, and their potential inter-relationships. In pursuing such an approach, it
612 is important to remember the different spectral biases in different proxy types – e.g.,
613 some proxies could be strongly correlated with PDO-related variability simply because
614 they are “climate integrators”, responding to ENSO-related forcing in the same way that
615 the North Pacific Ocean does (Newman et al. 2003; see also Pederson et al. 2011). As it

stands, the current disagreement amongst the existing PDO reconstructions is problematic for any assessment of PDO variability and PDO-related impacts over the last several hundred years (Kipfmueller et al. 2012).

6. Use of the PDO in climate diagnosis and prediction

In this section, we address both forecasting the PDO, and forecasting with the PDO, focusing on the need to distinguish between PDO-correlated and PDO-predictable climate impacts.

6.1 RETROSPECTIVE ANALYSIS OF PDO IMPACTS

PDO dependence on other climate processes implies that correlations with the PDO will be related to correlations with other climate indices. For example, Fig. 12 shows the correlation of revised United States climate division (nClimDiv; Vose et al 2014) cold-season precipitation (left panels) and temperature (right panels) anomalies with the PDO, ENSO, and NPI indices. While there are some interesting differences, the precipitation maps are all quite similar, with ENSO having the most pronounced signal. For cold-season temperatures (Fig. 12d-f), there are notable differences between the PDO and ENSO correlation patterns; however, now the PDO pattern is quite similar to, and somewhat weaker than, temperature correlations with the NPI. Since both ENSO and the NPI lead the PDO (Fig. 3), these results suggest that much of the PDO correlation patterns may not represent a direct response to the PDO. Repeating the analysis for the warm season (May-September) yields similar relationships between the correlation patterns, although all are somewhat weaker (not shown). A key concern then is to

637 determine *additional* predictive information from the PDO, and not merely duplicate
638 teleconnections from those processes that *simultaneously* act to force it.
639 Many studies that have explored historical PDO relationships with climate,
640 especially hydrological quantities including precipitation, snowpack, streamflow, and
641 drought (eg, Gershunov and Barnett 1998; Hamlet and Lettenmaier 1999; McCabe and
642 Dettinger 1999, 2002; Gutzler et al. 2002; Brown and Comrie 2004; McCabe et al. 2004;
643 Stewart et al. 2005; Hunter et al. 2006; Kurtzman and Scanlon 2007; Yu and Zwiers
644 2007; Higgins et al. 2007; Hu and Huang 2009; Zhang et al. 2010; Goodrich and Walker
645 2011; Mehta et al. 2012; Li et al. 2012; McCabe et al. 2012; Cook et al. 2014; Oakley and
646 Redmond 2014; Wang et al. 2014), are often focused on the impact of PDO phase on
647 ENSO teleconnections. However, sorting ENSO responses by PDO phase may have
648 unanticipated pitfalls beyond double counting the ENSO signal. On average, well over
649 half of the large-scale extratropical atmospheric seasonal-mean anomaly occurring during
650 an ENSO event is a consequence not of ENSO, but rather of ever-present weather and
651 internal slowly-evolving atmospheric anomalies such as blocking (e.g., Lau 1997). This
652 "ENSO-year/but-non-ENSO-forced" atmospheric anomaly also modifies North Pacific
653 SSTAs through changes in surface fluxes, while simultaneously contributing to the
654 seasonal-mean climate anomaly downstream over North America (Pierce 2002).
655 [Obviously, such anomalies exist in non-ENSO years as well; cf. NPI and PDO
656 temperature correlations in Fig. 12.] Additionally, like snowflakes no two ENSO events
657 are alike; recent research (see review by Capotondi et al. 2015) suggests that "diversity"
658 amongst ENSO events may also drive different and/or asymmetric teleconnections across
659 the North Pacific into North America (eg., Hoerling et al. 2001; Larkin and Harrison

660 2005; Wu et al. 2005; Mo 2010; Yu et al 2012). Of course, different teleconnections
661 could drive variations in the atmospheric bridge with consequent PDO variations (eg, An
662 et al. 2007; Yeh et al. 2015), including on decadal time scales (Yeh and Kirtman 2008).
663 ENSO diversity is evident in separate ENSO SST composites based on high/low PDO
664 years (see Fig. 13; also cf. the North Pacific SSTAs for the two ENSO eigenmodes in
665 Figs. 6d and f), raising the possibility that this stratification may partly capture ENSO
666 diversity impacts on both PDO and ENSO teleconnections, rather than PDO impacts on
667 ENSO teleconnections.

668 6.2 PDO PREDICTION

669 Interest in PDO prediction is high due to its potential climate impacts, especially
670 related to decadal variation and PDO regime shifts. From the earlier discussion, however,
671 we might expect that predicting regime duration, which may depend upon the current
672 amplitude of different processes with different memory time scales, could be more
673 skillful than predicting regime shifts, which may be largely randomly forced.

674 Some extended forecast skill resulting from oceanic Rossby wave propagation
675 (Schneider and Miller 2001) may occur for western Pacific SSTAs within the SAFZ.
676 Recent studies established multi-year predictability of the Kuroshio extension speed
677 (Nonaka et al. 2012; c.f. Nonaka et al. 2016) and stability (Qiu et al. 2014) that enter the
678 PDO forcing F in equation (1). How much this enhances PDO predictability (see Figs.
679 5a, 5b) remains to be determined, but it may be related to the more slowly evolving North
680 Pacific component in Fig. 6ab.

681 Given the PDO's relationship with ENSO, PDO forecast skill strongly depends on
682 ENSO forecast skill, especially for forecast leads of up to 1-2 years (eg, Alexander et al.

683 2008b; Wen et al. 2012). For longer forecast leads, largely unpredictable ENSO events
684 act mostly as high amplitude noise for decadal forecasts (Newman 2013; Wittenberg et
685 al. 2014). This may help explain why decadal PDO forecast skill in CMIP5 hindcasts,
686 which are initialized from the observed oceanic state, is unimpressive (Guemas et al.
687 2012; Kim et al. 2012; van Oldenborgh et al. 2012; Newman 2013; Meehl and Teng
688 2014), although model bias also contributes (Guemas et al. 2012; Kim et al. 2014).
689 Similarly, predicting the atmospheric impacts associated with the PDO may depend upon
690 tropical forecast skill. In fact, current GCM forecasts initialized with a PDO SSTA alone
691 have little atmospheric skill (Kumar et al. 2013; Kumar and Wang 2014), although
692 additional skill with higher resolution models remains possible (eg, Jung et al. 2012).

693 **7. The IPO and the PDO**

694 One particular pattern of ENSO-like decadal variability, the Interdecadal Pacific
695 Oscillation (IPO; Power et al. 1999; Folland et al. 2002; Parker et al. 2007; Dai 2012), is
696 often compared to the PDO. The precise definition of the IPO varies, but typically it has
697 been defined as the projection of monthly Pacific SST data upon a pattern representing
698 lowpass (~decadal) global SST variability (Parker et al. 2007; Henley et al. 2015). The
699 resulting IPO monthly time series (Henley et al. 2015) is essentially identical to the
700 leading PC of monthly Pacific basin SSTA variability, whether or not it has been lowpass
701 filtered (r = 0.99). Moreover, the unfiltered IPO time series is very highly correlated to
702 the ENSO PC used in Fig. 3 (r = 0.96), even when both are lowpass filtered (r=0.89).

703 However, the IPO is not identical to the PDO. While North and South Pacific
704 centers of action in the IPO regression pattern are roughly equivalent (eg, Henley et al.
705 2015), the PDO North Pacific center is significantly enhanced (Fig. 1a; see also the

orange circle in Fig. 2). Conversely, the South Pacific decadal oscillation (SPDO) (eg, Chen and Wallace 2015), the leading PC in the 20ºS-70ºS Pacific domain, has hemispheric asymmetry but with a South Pacific maximum in its regression pattern. The SPDO also has reemergence (during austral spring) and stronger ENSO forcing (Shakun and Shaman 2009). In fact, the SPDO and IPO time series are actually more correlated (r = 0.82) than the PDO and IPO time series (r = 0.74), although this difference diminishes with lowpass filtering. The PDO and SPDO unfiltered (lowpass) PCs are also correlated, but less highly than each is to the IPO and ENSO, with r = 0.5 (0.56).

It seems reasonable to suggest, based on the above correlations as well as the discussion in sections 2 and 3, that the IPO represents the reddened ENSO component, driven by both interannual and decadal ENSO variability, which is coherent between the North and South Pacific. The difference between the PDO and IPO is then due to internal North Pacific processes, primarily due to atmospheric noise forcing of the PDO, directly through anomalous surface fluxes and indirectly via westward-propagating Rossby waves that drive SST variability in the SAFZ. Seasonality differences between the PDO and SPDO, in sensitivity to ENSO forcing and in reemergence, might also play a role in PDO/IPO differences, as would South Pacific atmospheric noise forcing. Which index should be used for climate diagnosis or prediction may thus depend upon the problem at hand. Note that the previous discussion relating to double counting in diagnostic studies will also apply (perhaps even more strongly) when using both ENSO and the IPO as predictors.

8. Concluding remarks

The PDO is now a well-established climate index, frequently used in correlation analyses to suggest physical linkage between a particular variable of interest and North Pacific Ocean variability. As summarized in Fig. 14, the PDO represents not a single phenomenon but rather a combination of processes that span the Tropics and extratropics. It is therefore important to distinguish climate impacts *correlated* with the PDO from climate impacts that are *predictable* by the PDO. In this context, since much of the PDO represents the oceanic response to atmospheric forcing, care should be taken when using the PDO as a "forcing" function of non-oceanic responses without a convincing argument for the physical forcing mechanism. For example, claiming that PDO drives contemporaneous changes in rainfall over western North America may be more simply explained by both variables (PDO and rainfall) being driven by a common forcing function (Pierce 2002) such as diverse ENSO events and internal variability of the mid-latitude atmosphere. A "common forcing function" must therefore be considered as the first approximation for explaining a discovered simultaneous correlation between non-oceanic variables and PDO, including when reconstructing PDO-related variability into the past with proxy records. Caution is also needed when using the PDO together with other indices in analyses where the PDO depends upon those indices; determining which portion of the PDO, and/or which PDO process, is legitimately an “independent” predictor is an important first step. Still, it is important to reiterate that just as the PDO should not be assumed to be an independent predictor, neither should it be assumed to be entirely dependent upon other predictors.

749 Ultimately, climate models may offer the best hope for establishing links with the
750 PDO, because the historical record of PDO has limited degrees of freedom, a
751 consequence of PDO representing an "integrated in time" response to forcing. Of course,
752 the issues presented above still need consideration when analyzing model output.
753 Moreover, while a realistic balance of PDO processes must be simulated in CGCMs, it
754 appears that the current generation of models underestimates tropical forcing of the PDO
755 in the North Pacific Ocean. While models with particularly weak tropical-PDO
756 connections could still be useful for examining some aspects of internal North Pacific
757 Ocean dynamics (e.g., Zhong et al. 2008; Giannakis and Majda 2012; Zhang and
758 Delworth 2015) and possible feedback to the atmosphere (Taguchi et al. 2012), their
759 inability to capture realistic tropical interactions with the North Pacific may yield
760 problematic conclusions about the PDO and its role in the global climate system. In fact,
761 eqn. (4) may provide a diagnostic foundation for process-based analysis of CMIP6
762 CGCMs, since it tests not only how well ENSO variability is captured but also how
763 ENSO teleconnections and North Pacific memory and dynamical processes are
764 simulated.
765 This paper has focused on the PDO, but of course it is but one element of Pacific
766 decadal variability. Note that many of the caveats above should also be kept in mind
767 when considering other modes in the North Pacific. We have only just begun to touch
768 upon what this picture of the PDO as a sum of processes means for diagnosis of PDO-
769 related regional climate, ecological, and socioeconomic impacts; the reconstruction of the
770 PDO and its multidecadal impacts from proxy data over the last several hundred years;
771 and the relationship between the PDO and global mean temperature variations including

772 the recent global surface warming "hiatus". These issues will be explored in a
773 forthcoming companion paper.
774
775 *Acknowledgements*. The authors wish to thank Mike Wallace, Mike McPhaden, Sasha
776 Gershunov, Joe Barsugli, and an anonymous reviewer for helpful comments that
777 significantly improved this paper. MN was supported by NOAA/CPO (CDEP) and NSF
778 AGS CLD 1035325. MA and JDS acknowledge support from NOAA/CPO (ESM) and
779 NASA. CD and ASP acknowledge support from the NOAA MAPP program. NCAR is
780 sponsored by the National Science Foundation. AJM was supported by NSF
781 OCE1026607 and OCE1419306. SM and HN were supported in part by the Japanese
782 Ministry of Education, Culture, Sports Science and Technology (MEXT) through Grant-
783 in-Aid for Scientific Research 2205 in Innovative Areas. SM is also supported by JSPS
784 KAKENHI Grant Number 15H01606, 26287110, 26610146. HN is also supported by
785 MEXT through Grants-in-Aid 25287120 and 26241003 and through Arctic Challenge for
786 Sustainability Program, and by the Japanese Ministry of Environment through
787 Environment Research and Technology Department Fund 2-1503. NS was supported by
788 NSF1357015, Department of Energy, Office of Science, DOE-DESC000511 and
789 JAMSTEC-IPRC Joint Investigations.
790

REFERENCES

Alexander, M. A., 1990: Simulation of the response of the North Pacific Ocean to the anomalous atmospheric circulation associated with El Nino. *Clim. Dyn*., **5**, 53–65.

Alexander, M. A., 1992: Midlatitude atmosphere-ocean interaction during El Nino. Part I: The North Pacific Ocean, *J. Clim*., **5**, 944 – 958.

Alexander, M., 2010: Extratropical air-sea interaction, sea surface temperature variability, and the Pacific Decadal Oscillation. Vol. 189 of *Geophysical Monograph Series*, American Geophysical Union, Washington, D. C., 123–148.

Alexander, M., I. Bladé, M. Newman, J. R. Lanzante, N.-C. Lau, and J. D. Scott, 2002: The Atmospheric Bridge: The Influence of ENSO Teleconnections on Air–Sea Interaction over the Global Oceans. *J. Climate*, **15**, 2205–2231.

Alexander, M., A. Capotondi, A. Miller, F. Chai, R. Brodeur and C. Deser, 2008a: Decadal variability in the Northeast Pacific in a physical-ecosystem model: Role of mixed layer depth and trophic interactions. *Journal of Geophysical Research-Oceans,* **113**, C02017, doi:10.1029/2007JC004359.

Alexander, M. A., and C. Deser, 1995: A mechanism for the recurrence of wintertime midlatitude SST anomalies. *J. Phys. Oceanogr.*, **25**, 122–137.

Alexander, M. A., C. Deser, and M. S. Timlin, 1999: The re-emergence of SST anomalies in the North Pacific Ocean. *J. Climate*, **12**, 2419–2431.

Alexander, M. A., N.-C. Lau, and J. D. Scott, 2004: Broadening the atmospheric bridge paradigm: ENSO teleconnections to the North Pacific in summer and to the tropical west Pacific-Indian oceans over the seasonal cycle. In *Earth's Climate: The Ocean-*

Atmosphere Interaction, edited by Geophys. Monogr. Ser., vol. 147, edited by C. Wang, S.-P. Xie, and J. A. Carton, pp. 85– 104, AGU, Washington, D. C..

Alexander, M. A., L. Matrosova, C. Penland, J. D. Scott, and P. Chang, 2008b: Forecasting Pacific SSTs: Linear Inverse Model Predictions of the PDO. *J. Climate*, **21**, 385-402.

Alexander, M., and J. D. Scott, 2008: The Role of Ekman Ocean Heat Transport in the Northern Hemisphere Response to ENSO. *J. Climate*, **21**, 5688–5707, doi:10.1175/2008JCLI2382.1.

Alexander, M. A., M. S. Timlin, and J. D. Scott, 2001: Winter-to- winter recurrence of sea surface temperature, salinity and mixed layer depth anomalies. *Prog. Oceanogr.,* **49**, 41–61.

Alexander, M. A., D. J. Vimont, P. Chang, and J. D. Scott, 2010: The Impact of Extratropical Atmospheric Variability on ENSO: Testing the Seasonal Footprinting Mechanism using Coupled Model Experiments. *J. Climate*, **23**, 2885-2901.

An, S. I., J.-S. Kug, A. Timmermann, I.-S. Kang, and O. Timm, 2010: The Influence of ENSO on the Generation of Decadal Variability in the North Pacific. *J. Climate*, **20**, 667–680, doi:10.1175/JCLI4017.1.

Anderson, P.J., and J.F. Piatt, 1999: Community reorganization in the Gulf of Alaska following ocean climate regime shift. *Mar. Ecol. Prog. Ser.*, **189** (26), 117-123.

Ault, T., C. Deser, M. Newman, and J. Emile-Geay, 2013: Characterizing decadal to centennial variability in the equatorial Pacific during the last millennium. *Geophys. Res. Lett*, **40**, 3450-3456, doi:10.1002/grl.50647.

835 Baines, P.G., and C. K. Folland, 2007: Evidence for a Rapid Global Climate Shift across
836 the Late 1960s. *J. Climate*, **20**, 2721–2744.
837 Barlow, M., S. Nigam, and E. H. Berbery, 2001: ENSO, Pacific Decadal Variability, and
838 U.S. Summertime Precipitation, Drought, and Stream Flow. *J. Climate*, **14**, 2105–2128.
839 Barnett, T., D. W. Pierce, M. Latif, D. Dommonget, and R. Saravanan, 1999:
840 Interdecadal interactions between the tropics and the midlatitudes in the Pacific basin,
841 *Geophys. Res. Lett*., **26**, 615 – 618.
842 Barsugli, J. J. and D. S. Battisti, 1998: The basic effects of atmosphere-ocean thermal
843 coupling on midlatitude variability. *J. Atmos. Sci*., **55**, 477-493.
844 Beamish, R. J. and D.R. Bouillon, 1993: Pacific salmon production trends in relation to
845 climate. *Can. J. Fish. Aquat. Sci.*, **50**, 1002-1016.
846 Bellenger, H., É. Guilyardi, J. Leloup, M. Lengaigne, and J. Vialard, 2014: ENSO
847 representation in climate models: from CMIP3 to CMIP5. *Climate Dynamics*, **42**, 1999-
848 2018.
849 Beran, J., 1994: *Statistics for long-memory processes*. Chapman and Hall, New York, 315
850 pp.
851 Bhatt, U. S., M. A. Alexander, D. S. Battisti, D. D. Houghton, and L. M. Keller, 1998:
852 Atmosphere-ocean interaction in the North Atlantic: Near-surface climate variability. *J.*
853 *Clim*., **11**, 1615 – 1632.
854 Bi, H., W. T. Peterson, and P. T. Strub, 2011: Transport and coastal zooplankton
855 communities in the northern California Current system. *Geophys. Res. Lett*., **38**, L12607,
856 doi:10.1029/2011GL047927

857 Biondi, F., A. Gershunov, and D. R. Cayan, 2001: North Pacific Decadal Climate
858 Variability since 1661. *J. Climate*, 14, 5–10.
859 Bladé, I., 1997: The influence of midlatitude coupling on the low- frequency variability
860 of a GCM. Part I: No tropical SST forcing. *J. Clim*., **10**, 2087–2106.
861 Bond, N. A., J. E. Overland, M. Spillane, and P. Stabeno, 2003: Recent shifts in the state
862 of the North Pacific. *Geophys. Res. Lett*., **30**, 2183, doi:10.1029/2003GL018597.
863 Brown, D. P., and A. C. Comrie, 2004: A winter precipitation "dipole" in the western
864 United States associated with multidecadal ENSO variability. *Geophys. Res. Lett*, **31**,
865 L09203, doi:10.1029/2003GL018726.
866 Capotondi, A., M. A. Alexander, and C. Deser, 2003: Why are there Rossby wave
867 maxima at 108S and 138N in the Pacific?, *J. Phys. Oceanogr*., **33**, 1549 – 1563.
868 Capotondi, A., M. A. Alexander, C. Deser, and M. McPhaden, 2005: Anatomy and
869 Decadal Evolution of the Pacific Subtropical Cells. *J. Climate*, **18**, 3739-3758.
870 Capotondi, A., A. T. Wittenberg, M. Newman, E. Di Lorenzo, J.-Y. Yu, P. Braconnot, J.
871 Cole, B. Dewitte, B. Giese, E. Guilyardi, F.-F. Jin, K. Karnauskas, B. Kirtman, T. Lee, N.
872 Schneider, Y. Xue, and S.-W. Yeh, 2015: Understanding ENSO diversity. *Bull. Amer.*
873 *Meteor. Soc.*, **96**, 921-938.
874 Carton, J.A., and B.S. Giese, 2008: A reanalysis of ocean climate using Simple Ocean
875 Data Assimilation (SODA). *Mon. Wea. Rev.,* **136**, 2999-3017.
876 Cayan, D.R., 1992: Latent and sensible heat flux anomalies over the northern oceans: The
877 connection to monthly atmospheric circulation. *J. Clim*., **5**, 354–369.
878 Chelton, D. B., and R. E. Davis, 1982: Monthly mean sea level variability along the west
879 coast of North America. *J. Phys. Oceanogr*., **12**, 757 – 784.

880 Chen, X. Y., and J. M. Wallace, 2015: ENSO-like variability: 1900-2013. *J. Climate*, in
881 press.
882 Chiang, J. C. H., and D. J. Vimont, 2004: Analagous meridional modes of atmosphere-
883 ocean variability in the tropical Pacific and tropical Atlantic. *J. Climate*, **17**(21), 4143–
884 4158.
885 Chiba, S., E. Di Lorenzo, A. Davis, J. E. Keister, B. Taguchi, Y. Sasai, and H. Sugisaki,
886 2013: Large-scale climate control of zooplankton transport and biogeography in the
887 Kuroshio-Oyashio Extension region. *Geophys. Res. Lett.*, **40**, 5182–5187.
888 Clarke A.J. and S. Van Gorder, 1994: On ENSO Coastal Currents and Sea Levels. *J.*
889 *Phys. Oceanogr.*, **24**, 661–680. doi: http://dx.doi.org/10.1175/1520-
890 0485(1994)024<0661:OECCAS>2.0.CO;2
891 Compo, G., and P.D. Sardeshmukh, 2010: Removing ENSO-related variations from the
892 climate record. *J. Climate*, **23**, 1957-1978. DOI: 10.1175/2009JCLI2735.1
893 Conroy, J.L., K.M. Cobb, J. Lynch-Stieglitz, and P. Polissar, 2014: Constraints on the
894 salinity-oxygen isotope relationship in the central tropical Pacific Ocean. *Marine*
895 *Chemistry* doi: 10.1016/j.marchem.2014.02.001.
896 Cook, B. I., J. E. Smerdon, R. Seager, and E. R. Cook, 2014: Pan-Continental Droughts
897 in North America over the Last Millennium. *J. Climate*, **27**, 383–397, doi:10.1175/JCLI-
898 D-13-00100.1.
899 Cook, E. R., K. R. Briffa, D. M. Meko, D. A. Graybill, and G. Funkhouser, 1995: The
900 segment length curse in long tree-ring chronology development for paleoclimatic studies.
901 *Holocene*, **5**, 229–237.

902 Dai, A., 2012: The influence of the inter-decadal Pacific oscillation on US precipitation
903 during 1923–2010. *Clim Dyn*, doi:10.1007/s00382-012-1446-5.
904 Davis, R.E., 1976: Predictability of Sea Surface Temperature and Sea Level Pressure
905 Anomalies over the North Pacific Ocean. *J. Phys. Oceanogr.*, **6**, 249–266.
906 Deser, C., M. A. Alexander, and M. S. Timlin, 1996 : Upper ocean thermal variations in
907 the North Pacific during 1970-1991. *J. Climate*, **9**, 1840-1855.
908 Deser, C., M. A. Alexander, and M. S. Timlin, 1999: Evidence for wind-driven
909 intensification of the Kuroshio Current Extension from the 1970s to the 1980s. *J. Clim.*,
910 **12**, 1697–1706.
911 Deser, C., M. A. Alexander, and M. S. Timlin, 2003: Understanding the Persistence of
912 Sea Surface Temperature Anomalies in Midlatitudes. *J. Climate* **16**, 57–72.
913 Deser, C., and M. L. Blackmon, 1995: On the Relationship between Tropical and North
914 Pacific Sea Surface Temperature Variations. *J. Climate*, **8**, 1677–1680.
915 Deser, C., A. S. Phillips, M. A. Alexander, and B. V. Smoliak, 2014: Projecting North
916 American Climate over the next 50 years: Uncertainty due to internal variability. *J.*
917 *Climate*, 27, 2271-2296, doi: 10.1175/JCLI-D-13-00451.1.
918 Deser, C., A. S. Phillips, and J. W. Hurrell, 2004: Pacific Interdecadal Climate
919 Variability: Linkages between the Tropics and the North Pacific during Boreal Winter
920 since 1900. *J. Climate*, **17**, 3109–3124.
921 Deser, C., and M. Timlin, 1998: Atmosphere-ocean interaction on weekly timescales in
922 the North Atlantic and Pacific. *J. Climate*, 10, 393-408.
923 Deser, C., and Coauthors, 2012: ENSO and Pacific Decadal Variability in the
924 Community Climate System Model Version 4. *J. Climate*, **25**, 2622–2651,

925 doi:10.1175/JCLI-D-11-00301.1.

926 Di Lorenzo, E., N. Schneider, K. M. Cobb, P. J. S. Franks, K. Chhak, A. J. Miller, J. C.

927 McWilliams, S. J. Bograd, H. Arango, E. Curchitser, T. M. Powell and P. Riviere, 2008:

928 North Pacific Gyre Oscillation links ocean climate and ecosystem change. *Geophysical*

929 *Research Letters*, **35**(8), doi:10.1029/2007gl032838.

930 Di Lorenzo, K. M. Cobb, J. Furtado, N. Schneider, B. Anderson, A. Bracco, M. A.

931 Alexander, and D. Vimont, 2010: Central Pacific El Niño and decadal climate change in

932 the North Pacific. *Nature Geosciences*, 3 (11), 762-765, doi: 10.1038/NGEO984.

933 Di Lorenzo, E., and M.D. Ohman, 2013: A double-integration hypothesis to explain

934 ocean ecosystem response to climate forcing. *Proceedings Of The National Academy Of*

935 *Sciences*, **110** (7), 2496-2499.

936 D'Arrigo, R., R. Villalba, and G. Wiles, 2001: Tree-ring estimates of Pacific decadal

937 climate variability. *Clim Dyn*, **18**, 219–224, doi:10.1007/s003820100177.

938 D'Arrigo, R., and R. Wilson, 2006: On the Asian expression of the PDO. *Int. J. Climatol*,

939 **26**, 1607–1617, doi:10.1002/joc.1326.

940 D'Arrigo, R., R. Wilson, G. Wiles, K. Anchukaitis, O. Solomina, N. Davi, C. Deser, and

941 E. Dolgova, 2014: Tree‐ring reconstructed temperature index for coastal northern Japan:

942 implications for western North Pacific variability. *Int. J. Climatol*, n/a–n/a,

943 doi:10.1002/joc.4230.

944 Ebbesmeyer, C. C., D. R. Cayan, D. R. McLain, F. H. Nichols, D. H. Peterson, and K. T.

945 Redmond, 1991: 1976 step in the Pacific climate: Forty environmental changes between

946 1968–1975 and 1977–1985. Proc. Seventh Annual Pacific Climate Workshop, Asilomar,

947 CA, California Dept. of Water Research, 115–126.

948 Enfield, D. B., and J. S. Allen, 1980: On the structure and dynamics of monthly mean sea
949 level anomalies along the Pacific coast of North and South America. *J. Phys. Oceanogr.*,
950 **10**, 557 – 588.
951 Fairbanks, R. G., M. N. Evans, J. L. Rubenstone, R. A. Mortlock, K. Broad, M. D.
952 Moore, and C. D. Charles, 1997: Evaluating climate indices and their geochemical
953 proxies measured in corals. *Coral Reefs*, **16**(suppl.), S93 – S100.
954 Felis, T., A. Suzuki, H. Kuhnert, N. Rimbu, and H. Kawahata, 2010: Pacific Decadal
955 Oscillation documented in a coral record of North Pacific winter temperature since 1873.
956 *Geophys. Res. Lett.*, **37**, n/a–n/a, doi:10.1029/2010GL043572.
957 Fleming, S. W., 2009: Exploring the nature of Pacific climate variability using a "toy"
958 nonlinear stochastic model. *Can. J. Phys*, **87**, 1127–1131, doi:10.1139/P09-095.
959 Fleming, S. W., 2014: A non-uniqueness problem in the identification of power-law
960 spectral scaling for hydroclimatic time series. *Hydrological Sciences Journal*, **59**, 73–84,
961 doi:10.1080/02626667.2013.851384.
962 Folland, C. K., 2008: Interdecadal Pacific Oscillation Time Series. Web document
963 retrieved from http://www.iges.org/c20c/IPO_v2.doc.
964 Folland, C. K., J. A. Renwick, M. J. Salinger, and A. B. Mullan, 2002: Relative
965 influences of the Interdecadal Pacific Oscillation and ENSO on the South Pacific
966 Convergence Zone. *Geophys. Res. Lett*, **29**, 1643, doi:10.1029/2001GL014201.
967 Fraedrich, K., U. Luksch, and R. Blender, 2004: 1/*f* model for long-time memory of the
968 ocean surface temperature. *Phys. Rev. E*, **70**, 037301, doi:10.1103/PhysRevE.70.037301.
969 Frankignoul, C., and K. Hasselmann, 1977: Stochastic climate models. Part II:

970 Application to sea-surface temperature anomalies and thermocline variability. *Tellus*, **29**,
971 284–305.
972 Frankignoul, C., P. Müller, and E. Zorita, 1997: A Simple Model of the Decadal
973 Response of the Ocean to Stochastic Wind Forcing. *J. Phys. Oceanogr.*, **27**, 1533–1546.
974 Frankignoul, C., and R. W. Reynolds, 1983: Testing a dynamical model for mid-latitude
975 sea surface temperature anomalies. *J. Phys. Oceanogr*., **13**, 1131–1145.
976 Frankignoul, C., N. Sennechael, Y. Kwon, and M. Alexander, 2011: Influence of the
977 meridional shifts of the Kuroshio and the Oyashio Extensions on the atmospheric
978 circulation. *J. Climate*, **24**, 762–777.
979 Furtado, J. C., E. Di Lorenzo, N. Schneider, and N. A. Bond, 2011: North Pacific
980 Decadal Variability and Climate Change in the IPCC AR4 Models. *J. Climate*, **24**, 3049–
981 3067, doi:10.1175/2010JCLI3584.1.
982 Gargett, A. E., 1997: The optimal stability "window": a mechanism underlying
983 383 decadal fluctuations in North Pacific salmon stocks. *Fish. Oceanogr*. **6**, 1-9.
984 Gershunov, A., and T. P. Barnett, 1998: Interdecadal Modulation of ENSO
985 Teleconnections. *Bull. Amer. Meteor. Soc*, **79**, 2715–2725, doi:10.1175/1520-
986 0477(1998)079<2715:IMOET>2.0.CO;2.
987 Giannakis, D., and A. J. Majda, 2012: Limits of predictability in the North Pacific sector
988 of a comprehensive climate model. *Geophys. Res. Lett*, **39**, n/a–n/a,
989 doi:10.1029/2012GL054273.
990 Gill, A. E., 1982: Atmosphere-ocean Dynamics.
991 Goodrich, G. B., and J. M. Walker, 2011: The Influence of the PDO on Winter
992 Precipitation During High- and Low-Index ENSO Conditions in the Eastern United

993 States. *Physical Geography*, **32**, 295–312, doi:10.2747/0272-3646.32.4.295.
994 Graham, N. E., 1994: Decadal-scale climate variability in the 1970s and 1980s:
995 Observations and model results. *Climate Dyn*., **10**, 135–159.
996 Granger, C. W. J., 1980: Long memory relationships and the aggregation of dynamic
997 models. *Journal of Econometrics*, **14**, 227–238.
998 Gu, D., and S. G. H. Philander, 1997: Interdecadal climate fluctuations that depend on
999 exchanges between the tropics and extratropics. *Science*, **275**, 805 – 807.
1000 Guan, B., and S. Nigam, 2008: Pacific Sea Surface Temperatures in the Twentieth
1001 Century: An Evolution-Centric Analysis of Variability and Trend. *J. Climate*, **21**, 2790–
1002 2809, doi:10.1175/2007JCLI2076.1.
1003 Guemas, V., F. J. Doblas-Reyes, F. Lienert, Y. Soufflet, and H. Du, 2012: Identifying the
1004 causes of the poor decadal climate prediction skill over the North Pacific. *J. Geophys.*
1005 *Res*, **117**, n/a–n/a, doi:10.1029/2012JD018004.
1006 Gutzler, D. S., D. M. Kann, and C. Thornbrugh, 2002: Modulation of ENSO-Based
1007 Long-Lead Outlooks of Southwestern U.S. Winter Precipitation by the Pacific Decadal
1008 Oscillation. *Weather and Forecasting*, **17**, 1163–1172.
1009 Hamlet, A.F., and D.P. Lettenmaier, 1999: Columbia River streamflow forecasting based
1010 on ENSO and PDO climate signals. *J Water Res Pl*, **125**, 333-341.
1011 Hanawa, K., and S. Sugimoto, 2004: 'Reemergence' areas of winter sea surface
1012 temperature anomalies in the world's oceans. *Geophys. Res. Lett*., **31**, L10303,
1013 doi:10.1029/2004GL019904.
1014 Hasselmann, K., 1976: Stochastic climate models. Part I. Theory. *Tellus*, **28**, 474—485.

1015 Higgins, R. W., V. B. S. Silva, W. Shi, and J. Larson, 2007: Relationships between
1016 Climate Variability and Fluctuations in Daily Precipitation over the United States. *J.*
1017 *Climate*, **20**, 3561–3579, doi:10.1175/JCLI4196.1.
1018 Henley, B.J., J. Gergis, D.J. Karoly, S.B. Power, J. Kennedy, and C.K. Folland, 2015: A
1019 Tripole Index for the Interdecadal Pacific Oscillation. *Clim. Dyn*., DOI 10.1007/s00382-
1020 015-2525-1 .
1021 Hoerling, M. P., A. Kumar, and T. Xu, 2001: Robustness of the Nonlinear Climate
1022 Response to ENSO's Extreme Phases. *J. Climate*, **14**, 1277–1293.
1023 Hsieh, C.-H., S. M. Glaser, A. J. Lucas, and G. Sugihara, 2005: Distinguishing random
1024 environmental fluctuations from ecological catastrophes for the North Pacific Ocean.
1025 *Nature*, **435**, 336–340, doi:10.1038/nature03553.
1026 Hu, Z.-Z., and B. Huang, 2009: Interferential Impact of ENSO and PDO on Dry and Wet
1027 Conditions in the U.S. Great Plains. *J. Climate*, **22**, 6047–6065,
1028 doi:10.1175/2009JCLI2798.1.
1029 Ishii, M., A. Shouji, S. Sugimoto, and T. Matsumoto, 2005: Objective Analyses of Sea-
1030 Surface Temperature and Marine Meteorological Variables for the 20th Century using
1031 ICOADS and the Kobe Collection. *Int. J. Climatol*., **25**, 865-879.
1032 Iwasaka, N., and J. M. Wallace, 1995: Large scale air sea inter- action in the Northern
1033 Hemisphere from a view point of variations of surface heat flux by SVD analysis. *J.*
1034 *Meteorol. Soc. Jpn*., **73**, 781–794.
1035 Jones, P.D. et al., 2009: High-resolution paleoclimatology of the last millennium: a
1036 review of current status and future prospects. *Holocene* **19**(1), 3-49.

1037 Jung, T. and co-authors, 2012: High-resolution global climate simulations with the
1038 ECMWF model in Project Athena: Experimental design, model climate and seasonal
1039 forecast skill. *J. Climate*, **25**, 3155-3172.
1040 Kaplan, A., M. Cane, Y. Kushnir, A. Clement, M. Blumenthal, and B. Rajagopalan,
1041 1998: Analyses of global sea surface temperature 1856-1991. *Journal of Geophysical*
1042 *Research*, **103**, 18,567-18,589.
1043 Kay, J. E., C. Deser, A. Phillips, A. Mai, C. Hannay, G. Strand, J. Arblaster, S. Bates, G.
1044 Danabasoglu, J. Edwards, M. Holland, P. Kushner, J. -F. Lamarque, D. Lawrence, K.
1045 Lindsay, A. Middleton, E. Munoz, R. Neale, K. Oleson, L. Polvani, and M. Vertenstein,
1046 2015: The Community Earth System Model (CESM) Large Ensemble Project: A
1047 community resource for studying climate change in the presence of internal climate
1048 variability. *Bull. Amer. Met. Soc.*, 96, 1333–1349, doi: 10.1175/BAMS-D-13-00255.1.
1049 Keister, J.E., E. Di Lorenzo, C.A. Morgan, V. Combes, W.T. Peterson, 2011:
1050 Zooplankton species composition is linked to ocean transport in the Northern California
1051 Current. *Global Change Biology*, **17**, 2498-2511.
1052 Kelly, K.A., R.J. Small, R.M. Samelson, B. Qiu, T.M. Joyce, Y.-O. Kwon and M.F.
1053 Cronin, 2010: Western boundary currents and frontal air-sea interaction: Gulf Stream and
1054 Kuroshio Extension. *J. Climate*, **23**, 5644-5667.
1055 Keshner, M. S., 1982: 1/f Noise. *Proceedings of the IEEE*, **70**, 212.
1056 Kim, H.-M., P. J. Webster, and J. A. Curry, 2012: Evaluation of short-term climate
1057 change prediction in multi-model CMIP5 decadal hindcasts, *Geophys. Res. Lett.*, **39**,
1058 L10701, doi:10.1029/2012GL051644.

1059 Kim, H. M., Y. G. Ham, and A. A. Scaife, 2014: Improvement of initialized decadal
1060 predictions over the North Pacific Ocean by systematic anomaly pattern correction. *J.*
1061 *Climate*, **27** (13), 5148-5162.
1062 Kipfmueller, K. F., E. R. Larson, and S. St George, 2012: Does proxy uncertainty affect
1063 the relations inferred between the Pacific Decadal Oscillation and wildfire activity in the
1064 western United States? *Geophys. Res. Lett*, **39**, n/a–n/a, doi:10.1029/2011GL050645.
1065 Kleeman, R., J. P. McCreary, and B. A. Klinger, 1999: A mechanism for the decadal
1066 variation of ENSO. *Geophys. Res. Lett*., **26**, 1743 – 1747.
1067 Klein, S. A., D. L. Hartmann, and J. R. Norris, 1995: On the relationships among low-
1068 cloud structure, sea surface temperature, and atmospheric circulation in the summertime
1069 northeast Pacific. *J. Climate*, **8**, 1140–1155.
1070 Kumar, A., and H. Wang, 2014: On the potential of extratropical SST anomalies for
1071 improving climate predictions. *Clim Dyn*, 1–13, doi:10.1007/s00382-014-2398-8.
1072 Kumar, A., H. Wang, W. Wang, Y. Xue, and Z.-Z. Hu, 2013: Does Knowing the Oceanic
1073 PDO Phase Help Predict the Atmospheric Anomalies in Subsequent Months? *J. Climate*,
1074 **26**, 1268–1285, doi:10.1175/JCLI-D-12-00057.1.
1075 Kurtzman, D., and B. R. Scanlon, 2007: El Nino–Southern Oscillation and Pacific
1076 Decadal Oscillation impacts on precipitation in the southern and central United States:
1077 Evaluation of spatial distribution and predictions. *Water Resour. Res*., **43**, W10427,
1078 doi:10.1029/2007WR005863.
1079 Kushnir, Y., W. A. Robinson, I. Bladé, N. M. J. Hall, S. Peng, and R. Sutton, 2002:
1080 Atmospheric response to extratropical SST anomalies: Synthesis and evaluation. *J. Clim*.,
1081 **15**, 2205 – 2231.

1082 Kwon, Y., M. Alexander, N. Bond, C. Frankignoul, H. Nakamura, B. Qiu, and L.
1083 Thompson, 2010: Role of the Gulf Stream and Kuroshio–Oyashio systems in large-scale
1084 atmosphere–ocean interaction: A review. *J. Climate*, **23**, 3249–3281.
1085 Kwon, Y.-O., and C. Deser, 2007: North Pacific Decadal Variability in the Community
1086 Climate System Model Version 2. *J. Climate*, **20**, 2416–2433, doi:10.1175/JCLI4103.1.
1087 Kwon, Y.-O., C. Deser and C. Cassou, 2010: Coupled atmosphere-mixed layer ocean
1088 response to ocean heat flux convergence along the Kuroshio Current Extension. *Climate*
1089 *Dyn.*, DOI 10.1007/s00382-010-0764-8.
1090 Laepple, T., and P. Huybers, 2014: Global and regional variability in marine surface
1091 temperatures. *Geophys. Res. Lett*, **41**, 2528–2534, doi:10.1002/2014GL059345.
1092 Larkin, N. K., and D.E., Harrison, 2005: On the definition of El Niño and associated
1093 seasonal average U.S. weather anomalies. *Geophys. Res. Lett*., **32**, L13705,
1094 doi:10.1029/2005GL022738.
1095 Latif, M., and T. P. Barnett, 1994: Causes of decadal climate variability over the North
1096 Pacific and North America. *Science*, **266**, 634–637.
1097 Latif, M., and T. P. Barnett, 1996: Decadal climate variability over the North Pacific and
1098 North America: Dynamics and predictability. *J. Clim*., **9**, 2407–2423.
1099 Lau, N.-C., 1997: Interactions between global SST anomalies and the midlatitude
1100 atmospheric circulation. *Bulletin of the American Meteorological Society*, **78**, 21-33.
1101 Lau, N. C., and M. J. Nath, 1994: A modeling study of the relative roles of tropical and
1102 extratropical SST anomalies in the variability of the global atmosphere-ocean system. *J.*
1103 *Clim*., **7**, 1184–1207.

1104 Lau, N.-C., and M. J. Nath, 1996: The role of the "atmospheric bridge" in linking tropical
1105 Pacific ENSO events to extratropical SST anomalies. *J. Clim.*, **9**, 2036–2057.
1106 Lau, N.-C., and M. J. Nath, 2001: Impact of ENSO on SST variability in the North
1107 Pacific and North Atlantic: Seasonal dependence and role of extratropical air-sea
1108 coupling. *J. Clim.*, **14**, 2846–2866.
1109 Li, L., W. Li, and Y. Kushnir, 2012: Variation of the North Atlantic subtropical high
1110 western ridge and its implication to Southeastern US summer precipitation. *Clim Dyn*, **39**,
1111 1401–1412, doi:10.1007/s00382-011-1214-y.
1112 Li, Y., F. Wang, and Y. Sun, 2012: Low-frequency spiciness variations in the tropical
1113 Pacific Ocean observed during 2003–2012. *Geophys. Res. Lett.*, **39**, L23601,
1114 doi:10.1029/2012GL053971.
1115 Lienert, F., J. C. Fyfe, and W. J. Merryfield, 2011: Do Climate Models Capture the
1116 Tropical Influences on North Pacific Sea Surface Temperature Variability? *J. Climate*,
1117 **24**, 6203–6209, doi:10.1175/JCLI-D-11-00205.1.
1118 Lindegren, M., D.M. Checkley, T. Rouyer, A.D. MacCall, N.C. Stenseth, 2013: Climate,
1119 fishing, and fluctuations of sardine and anchovy in the California Current. *Proc. Nat.*
1120 *Acad. Sci.*, **110**, 13,672–13,677, http://dx.doi.org/10.1073/ pnas.1305733110.
1121 Liu, Z., and M. A. Alexander, 2007: Atmospheric Bridge, Oceanic Tunnel and Global
1122 Climatic Teleconnections. *Rev. Geophys.*, **45**, RG2005, doi:10.1029/2005RG000172.
1123 MacDonald, G. M., and R. A. Case, 2005: Variations in the Pacific Decadal Oscillation
1124 over the past millennium. *Geophys. Res. Lett*, **32**, L08703, doi:10.1029/2005GL022478.
1125 Mantua, N. J., S. R. Hare, Y. Zhang, J. M. Wallace, and R. C. Francis, 1997: A Pacific
1126 Interdecadal Climate Oscillation with Impacts on Salmon Production. *Bull. Amer.*

1127 *Meteor. Soc*, **78**, 1069–1079.

1128 McCabe, G. J., and M. D. Dettinger, 1999: Decadal variations in the strength of ENSO

1129 teleconnections with precipitation in the western United States. *Int. J. Climatol*, **19**,

1130 1399–1410.

1131 McCabe, G. J., and M. D. Dettinger, 2002: Primary Modes and Predictability of Year-to-

1132 Year Snowpack Variations in the Western United States from Teleconnections with

1133 Pacific Ocean Climate. *J. Hydrometeor*, **3**, 13–25.

1134 McCabe, G. J., M. A. Palecki, and J. L. Betancourt, 2004: Pacific and Atlantic Ocean

1135 influences on multidecadal drought frequency in the United States. *Proceedings of the*

1136 *National Academy of Sciences*, **101**, 4136–4141, doi:10.1073/pnas.0306738101.

1137 McCabe, G. J., T. R. Ault, B. I. Cook, J. L. Betancourt, and M. D. Schwartz, 2012:

1138 Influences of the El Niño Southern Oscillation and the Pacific Decadal Oscillation on the

1139 timing of the North American spring. *Int. J. Climatol*, **32**, 2301–2310,

1140 doi:10.1002/joc.3400.

1141 McCabe-Glynn, S., K. R. Johnson, C. Strong, M. Berkelhammer, A. Sinha, H. Cheng,

1142 and R. L. Edwards, 2013: Variable North Pacific influence on drought in southwestern

1143 North America since AD 854. *Nature Geosci*, **6**, 617–621, doi:10.1038/ngeo1862.

1144 McPhaden, M. J., and D. Zhang, 2002: Slowdown of the meridional overturning

1145 circulation in the upper Pacific Ocean. *Nature*, **415**, 603 – 608.

1146 Meehl, G. A., A. Hu, and B. D. Santer, 2009: The Mid-1970s Climate Shift in the Pacific

1147 and the Relative Roles of Forced versus Inherent Decadal Variability. *J. Climate*, **22**,

1148 780–792, doi:10.1175/2008JCLI2552.1.

1149 Meehl, G. A., and H. Teng, 2014: CMIP5 multi-model hindcasts for the mid-1970s shift

1150 and early 2000s hiatus and predictions for 2016–2035. *Geophys. Res. Lett*, **41**, 1711–
1151 1716, doi:10.1002/2014GL059256.
1152 Mehta, V. M., N. J. Rosenberg, and K. Mendoza, 2012: Simulated impacts of three
1153 decadal climate variability phenomena on dryland corn and wheat yields in the Missouri
1154 River Basin. *Agricultural and Forest Meteorology*, **152**, 109–124,
1155 doi:10.1016/j.agrformet.2011.09.011.
1156 Mestas-Nuñez, A. M., and D. B. Enfield, 1999: Rotated global modes of non-ENSO sea
1157 surface temperature variability, *J. Clim*., **12**, 2734–2746.
1158 Miller, A.J., D.R. Cayan, T.P. Barnett, N.E. Graham, and J.M. Oberhuber, 1994a: The
1159 1976-77 climate shift of the Pacific Ocean. *Oceanography* **7**(1), 21–26,
1160 http://dx.doi.org/10.5670/oceanog.1994.11.
1161 Miller, A. J., D. R. Cayan, T. P. Barnett, N. E. Graham, and J. M. Oberhuber, 1994b:
1162 Interdecadal variability of the Pacific Ocean: Model response to observed heat flux and
1163 wind stress anomalies. *Climate Dyn.,* **9,** 287–302.
1164 Miller, A. J. and N. Schneider, 2000: Interdecadal climate regime dynamics in the North
1165 Pacific Ocean: Theories, observations and ecosystem impacts. *Progress in*
1166 *Oceanography,* **47**, 355-379.
1167 Milotti, E., 1995: Linear processes that produce 1/*f* or flicker noise. *Phys. Rev. E.*, **51**,
1168 3087-3103.
1169 Minobe, S., 1997: A 50-70 year climatic oscillation over the North Pacific and North
1170 America. *Geophys. Res. Lett.*, **24**, pp 683-686.
1171 Minobe, S., 2012: Resonance in bidecadal and pentadecadal climate oscillations over the
1172 North Pacific: Role in climatic regime shifts. *Geophys. Res. Lett*, **26**, 855–858,

1173 doi:10.1029/1999GL900119.

1174 Miyasaka, T., H. Nakamura, B. Taguchi, and M. Nonaka, 2014: Multidecadal

1175 modulations of the low-frequency climate variability in the wintertime North Pacific

1176 since 1950. *Geophys. Res. Lett*., **41**, 2948–2955, doi:10.1002/2014GL059696.

1177 Miyasaka, T., and H. Nakamura, 2005: Summertime subtropical highs and tropospheric

1178 planetary waves in the Northern Hemisphere. *J. Climate*, **18**, 5046-5065.

1179 Mo, K. C., 2010: Interdecadal Modulation of the Impact of ENSO on Precipitation and

1180 Temperature over the United States. *J. Climate*, **23**, 3639–3656,

1181 doi:10.1175/2010JCLI3553.1.

1182 Nakamura, H., G. Lin, T. Yamagata, 1997: Decadal climate variability in the North

1183 Pacific during the recent decades. Bull. Amer. Meteor. Soc., 78, 2215-2225.

1184 Nakamura, H. and T. Yamagata, 1999: Recent decadal SST variability in the

1185 Northwestern Pacific and associated atmospheric anomalies. "Beyond El Niño: Decadal

1186 and Interdecadal Climate Variability". A. Navarra ed., Springer, 49-72.

1187 Nakamura, H., and A. S, Kazmin, 2003: Decadal changes in the North Pacific oceanic

1188 frontal zones as revealed in ship and satellite observations. *J. Geophys. Res.,* 108(C3),

1189 3078, doi:10.1029/1999JC000085.

1190 Nakamura, H., T. Sampe, Y. Tanimoto, and A. Shimpo, 2004: Observed associations

1191 among storm tracks, jet streams and midlatitude oceanic fronts, "Earth's Climate: The

1192 Ocean-Atmosphere Interaction", C. Wang, S.-P. Xie and J. A. Carton, Eds., Geophys.

1193 Monogr., **147**, American Geophysical Union, Washington, D.C., U.S.A., 329-346.

1194 Namias, J., and R. M. Born, 1970: Temporal coherence in North Pacific sea-surface

1195 temperature patterns, *J. Geophys. Res*., **75**, 5952 – 5955.

1196 Namias, J., and R. M. Born, 1974: Further studies of temporal coherence in North Pacific
1197 sea surface temperatures. *J. Geophys. Res*., **79**, 797–798.
1198 Newman, M., 2007: Interannual to Decadal Predictability of Tropical and North Pacific
1199 Sea Surface Temperatures. *J. Climate*, **20**, 2333–2356, doi:10.1175/JCLI4165.1.
1200 Newman, M., 2013: An empirical benchmark for decadal forecasts of global surface
1201 temperature anomalies. *J. Climate*, **26**, 5260-5269, doi:10.1175/JCLI-D-12-00590.1.
1202 Newman, M., G. P. Compo, and M. Alexander, 2003: ENSO-Forced Variability of the
1203 Pacific Decadal Oscillation. *J. Climate*, **16**, 3853–3857.
1204 Newman, M., P. D. Sardeshmukh, and C. Penland, 2009: How important is air-sea
1205 coupling in ENSO and MJO evolution? *J. Climate*, **22**, 2958-2977.
1206 Newman, M., S.-I. Shin, and M. A. Alexander, 2011: Natural variation in ENSO flavors.
1207 *Geophys. Res. Lett.,* **38**, L14705, doi:10.1029/2011GL047658.
1208 Nonaka, M., H. Nakamura, Y. Tanimoto, T. Kagimoto, and H. Sasaki, 2006: Decadal
1209 variability in the Kuroshio–Oyashio Extension Simulated in an Eddy-Resolving OGCM.
1210 *J. Climate*, **19**, 1970–1989, doi:10.1175/JCLI3793.1.
1211 Nonaka, M., H. Nakamura, Y. Tanimoto, T. Kagimoto, and H. Sasaki, 2008: Interannual-
1212 to-decadal variability in the Oyashio and its influence on temperature in the subarctic
1213 frontal zone: An eddy-resolving OGCM simulation. *J. Climate*, **21**, 6283–6303,
1214 doi:10.1175/2008JCLI2294.1.
1215 Nonaka, M., H. Sasaki, B. Taguchi, and H. Nakamura, 2012: Potential predictability of
1216 interannual variability in the Kuroshio Extension jet speed in an eddy-resolving OGCM.
1217 *J. Climate*, **25**, 3645-3652.

1218 Nonaka, M., Y. Sasai, H. Sasaki, B. Taguchi, and H. Nakamura, 2016: How potentially
1219 predictable are midlatitude ocean currents? *Sci. Rep.,* **6**, 20153, doi: 10.1038/srep20153.
1220 Norris, J. R., 1998: Low cloud type over the ocean from surface observations. Part II:
1221 Geographic and seasonal variations. *J. Climate*, **11**, 383–403.
1222 Norris, J. R., Y. Zhang, and J. M. Wallace, 1998: Role of clouds in summertime
1223 atmosphere-ocean interactions over the North Pacific. *J. Clim*., **11**, 2482–2490.
1224 Nurhati, I., K.M. Cobb, and E. Di Lorenzo, 2011: Decadal-scale SST and salinity
1225 variations in the central tropical Pacific: signatures of natural and anthropogenic climate
1226 change. *J. Climate*, doi: 10.1175/2011JCLI3852.1.
1227 O'Reilly, C. H., and A. Czaja, 2014: The response of the Pacific storm track and
1228 atmospheric circulation to Kuroshio Extension variability. *Quart. J. R. Meteor. Soc.,* **141***,*
1229 52-66, doi: 10.1002/qj.2334
1230 Oakley, N. S., and K. T. Redmond, 2014: A Climatology of 500-hPa Closed Lows in the
1231 Northeastern Pacific Ocean, 1948–2011. *J. Appl. Meteor. Climatol.*, **53**, 1578–1592,
1232 doi:10.1175/JAMC-D-13-0223.1.
1233 Okajima, S., H. Nakamura, K. Nishii, T. Miyasaka, and A. Kuwano-Yoshida, 2014:
1234 Assessing the importance of prominent warm SST anomalies over the midlatitude North
1235 Pacific in forcing large-scale atmospheric anomalies during 2011 summer and autumn. *J.*
1236 *Climate*, **27**, 3889–3903, doi:10.1175/JCLI-D-13-00140.1.
1237 Oldenborgh, G.J. van, F.J. Doblas-Reyes, B. Wouters and W. Hazeleger, 2012: Skill in
1238 the trend and internal variability in a multi-model decadal prediction ensemble. *Clim.*
1239 *Dyn.,* **38**, 1263-1280, doi:10.1007/s00382-012-1313-4.

1240 Oshima, K., and Y. Tanimoto, 2009: An evaluation of reproducibility of the Pacific
1241 decadal oscillation in the CMIP3 simulations. *J Meteorol Soc Japan*, **87**(4):755–770.
1242 Overland, J. E., J. Alheit, A. Bakun, J. W. Hurrell, D. L. Mackas, and A. J. Miller, 2010:
1243 Climate controls on marine ecosystems and fish populations. *Journal of Marine Systems*,
1244 **79**, 305–315, doi:10.1016/j.jmarsys.2008.12.009.
1245 Overland, J. E., D. B. Percival, and H. O. Mofjeld, 2006: Regime shifts and red noise in
1246 the North Paciifc. *Deep-Sea Research I*, **53**, 582-588.
1247 Park, J.-H., S. I. An, S.-W. Yeh, and N. Schneider, 2013: Quantitative assessment of the
1248 climate components driving the pacific decadal oscillation in climate models. *Theor Appl*
1249 *Climatol*., **112**, 431–445, doi:10.1007/s00704-012-0730-y.
1250 Parker, D., C. Folland, A. Scaife, J. Knight, A. Colman, P. Baines, and B. Dong, 2007:
1251 Decadal to multidecadal variability and the climate change background. *J. Geophys. Res*.,
1252 **112**, D18115, doi:10.1029/2007JD008411.
1253 Pederson, G. T., S. T. Gray, T. Ault, W. Marsh, D. B. Fagre, A. G. Bunn, C. A.
1254 Woodhouse, and L. J. Graumlich, 2011: Climatic Controls on the Snowmelt Hydrology
1255 of the Northern Rocky Mountains. *J. Climate*, **24**, 1666–1687,
1256 doi:10.1175/2010JCLI3729.1.
1257 Penland, C., and P. D. Sardeshmukh, 1995: The optimal growth of tropical sea surface
1258 temperature anomalies. *J. Climate*, **8**, 1999—2024.
1259 Penland, C., and P. D. Sardeshmukh, 2012: Alternative interpretations of power-law
1260 distributions found in nature. *Chaos*, **22**, 023119, doi:10.1063/1.4706504.
1261 Percival, D. B., J. E. Overland, and H. O. Mofjeld, 2001: Interpretation of North Pacific
1262 variability as a short- and long-memory process. *J. Climate*, **14**, 4545-4559.

1263 Phillips, A. S., C. Deser, and J. Fasullo, 2014: A New Tool for Evaluating Modes of
1264 Variability in Climate Models. *EOS*, **95**, 453-455, doi: 10.1002/2014EO490002.
1265 Pierce, D. W., 2001: Distinguishing coupled ocean–atmosphere interactions from
1266 background noise in the North Pacific. *Progress in Oceanography*, **49**, 331–352,
1267 doi:10.1016/S0079-6611(01)00029-5.
1268 Pierce, D. W., 2002: The Role of Sea Surface Temperatures in Interactions between
1269 ENSO and the North Pacific Oscillation. *J. Climate*, **15**, 1295–1308, doi:10.1175/1520-
1270 0442(2002)015<1295:TROSST>2.0.CO;2.
1271 Polade, S. D., A. Gershunov, D. R. Cayan, M. D. Dettinger, and D. W. Pierce, 2013:
1272 Natural climate variability and teleconnections to precipitation over the Pacific-North
1273 American region in CMIP3 and CMIP5 models. *Geophys. Res. Lett*, **40**, 2296–2301,
1274 doi:10.1002/grl.50491.
1275 Power, S., M. Haylock, R. Colman, and X. Wang, The Predictability of Interdecadal
1276 Changes in ENSO Activity and ENSO Teleconnections. *journals.ametsoc.org*.
1277 Power, S., T. Casey, C. Folland, A. Colman, and V. Mehta, 1999: Inter-decadal
1278 modulation of the impact of ENSO on Australia. *Clim Dyn*, **15**, 319–324,
1279 doi:10.1007/s003820050284.
1280 Rodgers, K. B., P. Friederichs, and M. Latif, 2004: Tropical Pacific decadal variability
1281 and its relation to decadal modulation of ENSO. *J. Climate*, **17**, 3761–3774.
1282 Qiu, B., 2000: Interannual variability of the Kuroshio extension system and its impact on
1283 the wintertime SST field. *J. Phys. Oceanogr.*, **30**, 1486-1502.
1284 Qiu, B., 2002: The Kuroshio Extension system: Its large-scale variability and role in the
1285 midlatitude ocean-atmosphere interaction. *J. Oceanogr.*, **58**, 57-75.

1286 Qiu, B., 2003: Kuroshio Extension variability and forcing of the Pacific decadal
1287 oscillations: Responses and potential feedback. *J. Phys. Oceanogr*., **33**, 2465–2482.
1288 Qiu, B., and S. Chen, 2005: Variability of the Kuroshio Extension Jet, Recirculation
1289 Gyre, and Mesoscale Eddies on Decadal Time Scales. *J. Phys. Oceanogr.*, **35**, 2090–
1290 2103.
1291 Qiu, B., and S. Chen, 2010: Eddy-mean flow interaction in the decadally-modulating
1292 Kuroshio Extension system. *Deep-Sea Res. II*, **57**, 1098-1110.
1293 Qiu, B., N. Schneider, and S. Chen, 2007: Coupled Decadal Variability in the North
1294 Pacific: An Observationally Constrained Idealized Model. *J. Climate*, **20**, 3602–3620,
1295 doi:10.1175/JCLI4190.1.
1296 Qiu, B., S. Chen, N. Schneider, and B. Taguchi, 2014: A Coupled Decadal Prediction of
1297 the Dynamic State of the Kuroshio Extension System. *J. Climate*, **27**, 1751–1764,
1298 doi:10.1175/JCLI-D-13-00318.1.
1299 Rayner, N. A., D. E. Parker, E. B. Horton, C. K. Folland, L. V. Alexander, D. P. Rowell,
1300 E. C. Kent, and A. Kaplan, 2003: Global analyses of sea surface temperature, sea ice, and
1301 night marine air temperature since the late nineteenth century. *J*. *Geophy Res*., **108**, 4407,
1302 doi:10.1029/2002JD002670.
1303 Reynolds, R. W., T. M. Smith, C. Liu, D. B. Chelton, K. S. Casey and M. G. Schlax,
1304 2007: Daily high-resolution blended analyses for sea surface temperature, *J. Climate*, **20**,
1305 5473-5496)
1306 Rudnick, D. L., and R. E. Davis, 2003: Red noise and regime shifts. *Deep Sea Research*
1307 *I*, **50**, 691-699.

1308 St George, S., 2014: An overview of tree-ring width records across the Northern
1309 Hemisphere. *Quaternary Science Reviews*, **95**, 132–150,
1310 doi:10.1016/j.quascirev.2014.04.029.
1311 Saravanan, R., and J. C. McWilliams, 1998: Advective ocean-atmosphere interaction: An
1312 analytical stochastic model with implications for decadal variability. *J. Climate*.
1313 Sardeshmukh, P.D., G.P. Compo, and C. Penland, 2000: Changes of probability
1314 associated with El Niño. *J. Climate*, 13, 4268-4286.
1315 Sasaki, Y. N., S. Minobe and N. Schneider, 2013: Decadal response of the Kuroshio
1316 Extension jet to Rossby waves: Observation and thin-jet theory. *J. Phys. Ocean*, **43**, 442-
1317 456.
1318 Sasaki, Y. N., and N. Schneider, 2011: Decadal shifts of the Kuroshio Extension jet:
1319 Application of thin-jet theory. *J. Phys. Ocean*., **41**, 979-993.
1320 Sasaki, Y. N., N. Schneider, N. Maximenko, and K. Lebedev, 2010: Observational
1321 evidence for propagation of decadal spiciness anomalies in the North Pacific, *Geophys.*
1322 *Res. Lett.*, **37**, L07708, doi:10.1029/2010GL042716.
1323 Schindler, D.E., L.A. Rogers, 2009: Responses of salmon populations to climate variation
1324 in freshwater ecosystems. Pages 1127-1142 in CG Krueger, CE Zimmerman (eds),
1325 Arctic-Yukon-Kuskokwim Sustainable Salmon Initiative. Am. Fish. Soc. Symp.
1326 Schneider, N., A. J. Miller, M. A. Alexander, and C. Deser, 1999: Subduction of decadal
1327 north Pacific temperature anomalies: Observations and dynamics. *J. Phys. Oceanogr*., **29**,
1328 1056 – 1070.
1329 Schneider, N., and A. J. Miller, 2001: Predicting Western North Pacific Ocean Climate.
1330 *J. Climate*, **14**, 3997–4002.

1331 Schneider, N., A. J. Miller, and D. W. Pierce, 2002: Anatomy of North Pacific Decadal
1332 Variability. *J. Climate*, **15**, 586–605.
1333 Schneider, N., and B. D. Cornuelle, 2005: The Forcing of the Pacific Decadal Oscillation.
1334 *J. Climate*, **18**, 4355–4373, doi:10.1175/JCLI3527.1.
1335 Schwartz, R.E., A. Gershunov, S.F. Iacobellis and D.R. Cayan, 2014: North American
1336 west coast summer low cloudiness: Broad scale variability associated with sea surface
1337 temperature. *Geophys. Res. Lett*., **41**, 3307-3314, DOI: 10.1002/2014GL059825.
1338 Seager, R., A. R. Karspeck, M.A. Cane, Y. Kushnir, A. Giannini, A. Kaplan, B. Kerman,
1339 and J. Velez, 2004: Predicting Pacific decadal variability. In *Earth's Climate: The*
1340 *Ocean-Atmosphere Interaction*, Geophysical Monograph Series 147, 105-120.
1341 Seager, R., Y. Kushnir, N. H. Naik, M. A. Cane, and J. Miller, 2001: Wind-Driven Shifts
1342 in the Latitude of the Kuroshio–Oyashio Extension and Generation of SST Anomalies on
1343 Decadal Timescales. *J. Climate*, **14**, 4249–4265.
1344 Shakun, J. D., and J. Shaman, 2009: Tropical origins of North and South Pacific decadal
1345 variability. *Geophys. Res. Lett*, **36**, L19711, doi:10.1029/2009GL040313.
1346 Sheffield, J., and Coauthors, 2013: North American Climate in CMIP5 Experiments. Part
1347 II: Evaluation of Historical Simulations of Intraseasonal to Decadal Variability. *J.*
1348 *Climate*, **26**, 9247–9290, doi:10.1175/JCLI-D-12-00593.1.
1349 Shen, C., W.-C. Wang, W. Gong, and Z. Hao, 2006: A Pacific Decadal Oscillation record
1350 since 1470 AD reconstructed from proxy data of summer rainfall over eastern China.
1351 *Geophys. Res. Lett.*, **33**, L03702, doi:10.1029/2005GL024804.

1352 Smirnov, D., M. Newman, and M. A. Alexander, 2014: Investigating the role of ocean-
1353 atmosphere coupling in the North Pacific Ocean. *J. Climate*, **27**, 592-606,
1354 doi:10.1175/JCLI-D-13-00123.1.
1355 Smirnov, D., M. Newman, M. A. Alexander, Y.-O. Kwon, and C. Frankignoul, 2015:
1356 Investigating the local atmospheric response to a realistic shift in the Oyashio sea surface
1357 temperature front. *J. Climate*, **28**, 1126-1147.
1358 Smith, T.M., R.W. Reynolds, T.C. Peterson, and J. Lawrimore, 2008: Improvements to
1359 NOAA's Historical Merged Land–Ocean Temp Analysis (1880–2006). *Journal of*
1360 *Climate*, **21**, 2283–2296.
1361 Stachura, M., N.J. Mantua, and M. Scheuerrell, 2014: Oceanographic influences on
1362 patterns in North Pacific salmon abundance. *Canadian Journal of Fisheries and Aquatic*
1363 *Sciences*, **71**(2): 226-235, 10.1139/cjfas-2013-0367.
1364 Steele, J. H., 2004: Regime shifts in the ocean: reconciling observations and theory.
1365 *Progress in Oceanography*, **60**, 135–141, doi:10.1016/j.pocean.2004.02.004.
1366 Strong, C., and G. Magnusdottir, 2009: The Role of Tropospheric Rossby Wave Breaking
1367 in the Pacific Decadal Oscillation. *J. Climate*, **22**, 1819–1833,
1368 doi:10.1175/2008JCLI2593.1.
1369 Sugimoto S., and K. Hanawa, 2011: Roles of SST anomalies on the wintertime turbulent heat
1370 fluxes in the Kuroshio-Oyashio Confluence Region: influences of warm eddies detached
1371 from the Kuroshio Extension. *J. Climate, **24***, 6551-6561.
1372 Taguchi, B., S.-P. Xie, N. Schneider, M. Nonaka, H. Sasaki, and Y. Sasai, 2007: Decadal
1373 variability of the Kuroshio Extension: Observations and an eddy-resolving model
1374 hindcast. *J. Climate*, **20**, 2357-2377.
1375 Taguchi, B., H. Nakamura, M. Nonaka, N. Komori, A. Kuwano-Yoshida, K. Takaya, and

1376 A. Goto, 2012: Seasonal Evolutions of Atmospheric Response to Decadal SST
1377 Anomalies in the North Pacific Subarctic Frontal Zone: Observations and a Coupled
1378 Model Simulation. *J. Climate*, **25**, 111–139, doi:10.1175/JCLI-D-11-00046.1.
1379 Takahashi, K., A. Montecinos, K. Goubanova, and B. Dewitte, 2011: ENSO regimes:
1380 Reinterpreting the canonical and Modoki El Niño. *Geophys. Res. Lett.,* **38**, L10704,
1381 doi:10.1029/2011GL047364.
1382 Takasuka, A., Y. Oozeki, H. Kubota, S. E. Lluch-Cota, 2008: Contrasting spawning
1383 temperature optima: Why are anchovy and sardine regime shifts synchronous across the
1384 North Pacific? *Progress In Oceanography*, **77**(2), 225-232.
1385 Tanimoto, Y., H. Nakamura, T. Kagimoto, and S. Yamane, 2003: An active role of
1386 extratropical sea surface temperature anomalies in determining anomalous turbulent heat
1387 fluxes. *J. Geophys. Res*., **108**(C10), 3304, doi:10.1029/2002JC001750
1388 Taylor, K. E., 2001: Summarizing multiple aspects of model performance in a single
1389 diagram. *J. Geophys. Res.,* **106**(D7), 7183–7192.
1390 Timlin, M. S., M. A. Alexander, and C. Deser, 2002: On the reemergence of North
1391 Atlantic SST anomalies. *J. Clim*., **15**, 2707 – 2712.
1392 Tingley, M. P., P. F. Craigmile, M. Haran, B. Li, E. Mannshardt, and B. Rajaratnam,
1393 2012: Piecing together the past: Statistical insights into paleoclimatic reconstructions.
1394 *Quat. Sci. Rev.*, **35**(0), 1–22, doi:10.1016/ j.quascirev.2012.01.012.
1395 Trenberth, K. E., G. W. Branstator, D. Karoly, A. Kumar, N.-C. Lau, and C. Ropelewski,
1396 1998: Progress during TOGA in understanding and modeling global teleconnections
1397 associated with tropical sea surface temperatures. J. *Geophys. Res*., **103**, 14,291 – 14,324.

1398 Trenberth, K. E., and D. P. Stepaniak, 2001: Indices of El Nino Evolution. *J. Climate*, **14**,
1399 1697-1701.
1400 Vimont, D. J. 2005: The contribution of the interannual ENSO cycle to the spatial pattern
1401 of decadal ENSO-like variability. *J. Climate*, **18**, 2080-2092.
1402 Vimont, D. J., M. Alexander, and A. Fontaine, 2009: Mid-latitude excitation of tropical
1403 variability in the Pacific: the role of thermodynamic coupling and seasonality. *J. Climate*,
1404 22, 518-534.
1405 Vimont, D. J., D. S. Battisti, and A. C. Hirst, 2001: Footprinting: a seasonal link between
1406 the mid-latitudes and tropics. Geophys. Res. Lett., 28(20), 3923–3926.
1407 Vimont, D. J., J. M. Wallace, and D. S. Battisti, 2003: The seasonal footprinting
1408 mechanism in the Pacific: Implications for ENSO, J. Clim., 16, 2668–2675,
1409 doi:10.1175/1520-0442(2003)0162.0.CO;2.
1410 Vose, R. S., and Coauthors, 2014: Improved Historical Temperature and Precipitation
1411 Time Series for U.S. Climate Divisions. *http://dx.doi.org/10.1175/JAMC-D-13-0248.1*,
1412 53, 1232–1251, doi:10.1175/JAMC-D-13-0248.1.
1413 Walker, G.T. and E.W. Bliss, 1932: World Weather V. *Memoirs of the Royal*
1414 *Meteorological Society*, **4**, (36), 53-84.
1415 Wang, H., A. Kumar, W. Wang, and Y. Xue, 2012: Seasonality of the Pacific Decadal
1416 Oscillation. *J. Climate*, **25**, 25–38.
1417 Wang, S.-Y., M. L'Heureux, and H-H Chia, 2012: ENSO prediction one year in advance
1418 using Western North Pacific sea surface temperatures. *Geophys. Res. Lett.*, 39, L05702
1419 Wang, S., J. Huang, Y. He, and Y. Guan, 2014: Combined effects of the Pacific Decadal
1420 Oscillation and El Niño-Southern Oscillation on Global Land Dry–Wet Changes.

1421 *Scientific Reports*, **4**, 6651, doi:10.1038/srep06651.

1422 Wen, C., A. Kumar, and Y. Xue, 2014: Factors contributing to uncertainty in Pacific

1423 Decadal Oscillation index. *Geophys. Res. Lett*, **41**, 7980–7986,

1424 doi:10.1002/2014GL061992.

1425 Wen, C., Y. Xue, and A. Kumar, 2012: Seasonal Prediction of North Pacific SSTs and

1426 PDO in the NCEP CFS Hindcasts. *J. Climate*, **25**, 5689–5710, doi:10.1175/JCLI-D-11-

1427 00556.1.

1428 Wittenberg, A.T., A. Rosati, T. L. Delworth, G. A. Vecchi, and F. Zeng, 2014: ENSO

1429 Modulation: Is It Decadally Predictable?. *J. Climate*, **27**, 2667–2681.

1430 Wood, R., 2012: Stratocumulus clouds. *Mon. Wea. Rev.,* **140**, 2373–2423.

1431 Wu, A., W. W. Hsieh, and A. Shabbar, 2005: The Nonlinear Patterns of North American

1432 Winter Temperature and Precipitation Associated with ENSO. *J. Climate*, **18**, 1736–

1433 1752, doi:10.1175/JCLI3372.1.

1434 Wu, L., Z. Liu, R. Gallimore, R. Jacob, D. Lee, and Y. Zhong, 2003: Pacific Decadal

1435 Variability: The Tropical Pacific Mode and the North Pacific Mode. *J. Climate*, **16**,

1436 1101–1120.

1437 Yeh, S.-W., and B. P. Kirtman, 2008: The Low-Frequency Relationship of the Tropical–

1438 North Pacific Sea Surface Temperature Teleconnections. *J. Climate*, **21**, 3416–3432,

1439 doi:10.1175/2007JCLI1648.1.

1440 Yeh, S.-W., X. Wang, C. Wang, and B. Dewitte, 2015: On the Relationship between the

1441 North Pacific Climate Variability and the Central Pacific El Niño. *J. Climate*, **28**, 663–

1442 677, doi:10.1175/JCLI-D-14-00137.1.

1443 Yim, B. Y., M. Kwon, H. S. Min, and J.-S. Kug, 2014: Pacific Decadal Oscillation and its

relation to the extratropical atmospheric variation in CMIP5. *Clim Dyn*, 1–20, doi:10.1007/s00382-014-2349-4.

Yu, B., and F. W. Zwiers, 2007: The impact of combined ENSO and PDO on the PNA climate: a 1,000-year climate modeling study. *Clim Dyn*, **29**, 837–851, doi:10.1007/s00382-007-0267-4.

Yu, J.-Y., Y. Zou, S. T. Kim, and T. Lee, 2012: The Changing Impact of El Nino on US Winter Temperatures. *Geophys. Res. Lett.*, doi:10.1029/2012GL052483

Zhang, D., and M J. McPhaden, 2006: Decadal variability of the shallow Pacific meridional overturning circulation: Relation to tropical sea surface temperatures in observations and climate change models. *Ocean Modelling*, **15**, 250-273.

Zhang, X., J. Wang, F. W. Zwiers, and P. Y. Groisman, 2010: The Influence of Large-Scale Climate Variability on Winter Maximum Daily Precipitation over North America. *J. Climate*, **23**, 2902–2915, doi:10.1175/2010JCLI3249.1.

Zhang, Y., J. M. Wallace, and D. S. Battisti, 1997: ENSO-like Interdecadal Variability: 1900–93. *J. Climate*, doi:10.1175/1520-0442(1997)010<1004:ELIV>2.0.CO;2.

Zhong, Y., Z. Liu, and R. Jacob, 2008: Origin of Pacific Multidecadal Variability in Community Climate System Model, Version 3 (CCSM3): A Combined Statistical and Dynamical Assessment. *J. Climate,* **21**, 114-133.

Table 1. Paleo reconstructions of the PDO used in Fig.5. Paleoclimate reconstructions were all obtained from the NOAA Paleoclimatology program and are publicly available. Each PDO reconstruction targets slightly different aspects of the PDO, and each follows its own conventions for normalization, so all indices are normalized to unit variance over the period 1901-2000.

Reconstruction	Time period	Proxies used	Season Targeted
Biondi et al. 2001	1661-1991	Tree-ring	ONDJFM*
D'Arrigo and Wilson 2006	1565-1988	Tree-Ring	MAM
MacDonald 2005	993-1996	Tree-Ring	Annual (Jan-Dec)
D'Arrigo et al. 2001	1700-1979	Tree-Ring	NDJFM*
Felis et al. 2010	1873-1994	Coral (Porites)	NDJF
Shen et al. 2006	1470-1998	Historical Docs	Annual

1478

FIGURE CAPTIONS

Figure 1. The Pacific decadal oscillation (PDO) over the historical record (1901-2014). (a) Regression of global monthly SST (shading) and DJF SLP (contours; interval is 1 hPa) anomalies onto the PDO time series from the HadISST dataset. Note that a *positive* PDO is associated with *negative* central North Pacific SSTA. (b) PDO index time series determined from the SST datasets, COBE (Ishii et al. 2005), ERSSTv3b (Smith et al. 2008), HadISST (Rayner et al. 200x), and Kaplan (Kaplan et al. 1998). The thick black line in each panel shows the smoothed (6-yr lowpass; Zhang et al. 1997) time series. The last panel shows the departure of each time series from the mean of all four time series. (c) Seasonal cycle of (3-month running mean) PDO index autocorrelation. Contour (shading) interval is 0.2 (0.1). Only values that are 95% significant are shaded. The month ordinate indicates the time of the PDO base month, and the lag indicates how far ahead/behind the PDO is; so, for example, the value plotted at (5, MAY) represents the correlation between the May value of the PDO and the subsequent October value of the PDO.

Figure 2. Taylor diagram (Taylor et al. 2001) comparing the reference PDO (HadISST) pattern (Fig. 1a, black circle) with variations due to sampling, observational dataset, and geographical domain; and to PDOs determined from CGCMs run with historical radiative forcing. In this diagram, the distance of a point from the origin is the pattern standard deviation normalized by the reference pattern standard deviation, and the distance from the reference point (at [0.26,0]) is the root mean square (rms) error normalized by the reference pattern standard deviation, indicated by the dashed semicircles spaced at an interval of 0.5. The pattern correlation, decreasing in a counterclockwise azimuthal

direction, is mathematically related to these two quantities. The analysis is taken only over the North Pacific PDO domain (20°N-70°N). Black dots: PDO estimates based on the 50yr Monte Carlo subsamples; triangles: PDO determined from the ERSSTv3b (blue), COBE (green), and Kaplan (magenta) observed data sets; orange symbols: SSTA structure (within the North Pacific PDO region) associated with the leading SSTA EOF, where the southern border of the Pacific domain is instead 0º (square), 20ºS (diamond), and 70ºS (circle). Also shown are the CMIP3 (cyan), CMIP5 (red), and CESM-LE (yellow) historical simulation PDOs. EOF spatial patterns were interpolated to the 2° by 2° grid used for the reference pattern. Due to differences in landmasks, metrics for the Taylor diagram were calculated over ocean points that were in common between each model and the HadISST data.

Figure 3. Illustration of how both local and remote atmospheric forcing can drive PDO variability. (a) One-season lead correlation between NDJ NPI and global SSTAs during FMA. (b) Seasonal cycle of cross correlation between the NPI and the PDO index (both filtered with 3-month running mean). PDO leads NPI for positive lags; NPI leads PDO for negative lags. In both panels (a) and (b), the NPI index sign has been flipped so that "positive" refers to a deepening of the Aleutian low, which also will correspond to positive PDO. (c) One-season lag correlation between the NDJ value of the "ENSO index" (the leading PC of tropical Pacific SSTA) and global SSTAs during FMA. (d) Seasonal cycle of cross correlation between the ENSO and PDO indices (both filtered with 3-month running mean). PDO leads ENSO for positive lags; ENSO leads PDO for negative lags. All figures are determined from 1901-2014 data; shading interval is 0.1. For panels (b) and (d), only values that are 95% significant are shaded, and the contour

line interval is 0.2. The month ordinate indicates the time of the PDO index base month, and the lag indicates how far ahead/behind the second variable is; so, for example, the value plotted at (5, MAY) represents the correlation between the May value of the PDO and the subsequent October value of the other variable.

Figure 4. Illustration of re-emergence of oceanic thermal anomalies. Correlation of the JFM value of the PDO index (as in Fig. 1b except determined from 3-month running means) with ECMWF ORAS4 ocean temperatures (Balmaseda et al. 2013) for the subsequent two years, area averaged in (a) the Gulf of Alaska, (b) the central Pacific, and (c) the west Pacific, for the years 1958-2014. The gray line shows the climatological mean mixed layer depth as a function of time of year at each location, so it repeats over the three year period.

Figure 5. Illustration of the slow ocean (Rossby wave) dynamics process driving PDO variability. (a) Time series of the SSTA in the mixed water region (MWR, solid) and the PDO index (dashed, with sign inverted). The temperature index is based on the optimal interpolation, blended, quarter degree SST analysis of Reynolds et al. (2007). The MWR extends from the coast of Japan to 150E, and between 36N to 42N. Both the MWR and PDO indices have been normalized by their respective standard deviation. The correlation between MWR and PDO indices is -0.49. (b) Satellite observed sea surface height anomalies in cm, averaged between 33N and 35N. The dotted line marks a westward phase speed of 3.7 cm/s (Qiu and Chen 2010). Sea surface temperature and sea surface height anomalies have been detrended and smoothed with a two year running mean, with weights varying linearly as a function of lag.

Figure 6. Reconstructing the PDO as the sum of three different dynamical processes. (a-h) Contributions to the PDO from (a) the second ("North Pacific"; Fig. 6b), (c) third ("Central Pacific ENSO"; Fig. 6d) and (e) fourth ("Eastern Pacific ENSO"; Fig. 6f shows most energetic phase of this complex eigenmode [essentially, cosine phase], with least energetic phase [sine phase] not shown) eigenmodes of the LIM described in the paper. Note that unlike EOFs, these eigenmodes are nonorthogonal. Contour interval is the same in all three eigenmode panels; all eigenmodes are normalized to have unit amplitude. The LIM is determined in a reduced EOF space (with 25 degrees of freedom) that retains about 85% of the SST variance in the Tropics and North Pacific deomains. (d) "PDO reconstruction", the sum of the time series shown in panels a, c, and e. (h) PDO index time series (same as Fig. 1c but with three-month running mean smoothing applied). In the time series panels, heavy black lines represent the application of the same 6-yr lowpass smoother as in Fig. 1b, and vertical green lines indicate times of PDO "regime shifts".

Figure 7. Epoch difference maps, showing SST differences between two adjacent 20 year means centered on (a) 1968/69 and (b) 1976/77. The adjacent 20-year periods used for each epoch calculation are indicated by the corresponding color bars in Fig. 6h.

Figure 8. The PDO over the historical record as simulated by coupled CGCMs. (a and b) Same as Fig. 1a except showing two selected members of the "historical" CMIP5 ensemble that are (a) closest and (b) farthest from the reference pattern in Fig. 2. (c and d) Same as Fig. 8a except showing two selected members of the CESM-LE that are (c) closest and (d) farthest from the reference pattern in Fig. 2. (e) PDO time series from all ensemble members; all time series are smoothed with the Zhang et al. filter (used in Fig.

1c). Thin gray lines represent each ensemble member, the thin black solid (dashed) line in the CMIP5 panel represents model A (B), and the thick black line is the ensemble mean for each set of models.

Figure 9. Temporal relationships relevant to the PDO for the CMIP3 (top row), CMIP5 (middle row), and LENS (bottom row) ensembles. Shown are: (a, d, g) the autocorrelation of the monthly PDO index; (b, e, h) the lagged seasonal correlation between the seasonal PDO index and the DJF averaged Nino 3.4 index; and (c, f, i) the lagged seasonal correlation between the seasonal PDO index and the DJF averaged PNA index. On all plots thin grey lines indicate model correlations, the thick solid black line indicates correlations for indices from the HadISST data, and the thick dashed line indicates correlations with indices from the ERSSTv3b data. For panels (c, f, i) the observed DJF PNA time series is obtained from the 20th Century Reanalysis. Observed correlations are taken over the time period 1901-2009, CMIP3 over 1900-1999, CMIP5 over 1901-2004, and LENS over 1920-2005. For seasonal correlations, positive lags indicate that the Nino 3.4 or PNA index leads the seasonal PDO index, and the label on the abscissa indicates the season for which the PDO is defined.

Figure 10. Parameters for an AR-1 model of the PDO time series, $PDO(n)=r\ PDO(n-1) + a\ ENSO1(n) + b\ ENSO2(n) + \varepsilon$, for CMIP5 models (blue bars) and observations (red bars). The AR-1 model is determined from the PDO index and two leading tropical PCs, ENSO1 and ENSO2, calculated as discussed in the text but for the period 1900 to 2000, and then averaged from July to June. (a) Unforced lag-1 auto correlation, i.e., r in the above equation. (b) Forcing coefficient for ENSO1, i.e., a in the above equation. (c) Forcing coefficient for ENSO2, i.e., b in the above equation. (d) Correlation ρ between

each model's PDO index time series and the corresponding estimated PDO timeseries determined from the AR-1 model.

Figure 11. Comparison of observed, paleoclimate, and CMIP5 PDO spectra: (a) CMIP5 "historical" simulations (190 runs total) and forced "last millennium" (past 1000 yrs) simulations (6 runs); (b) unforced "control" simulations (48 runs total); and (c) paleoclimate (tree ring and other proxy-based) reconstructions of the PDO. In panels (a-c), the thick black line represents the HadISST PDO spectrum, and the three thin blacks lines the other three observational PDO spectra. In each case, only winter (NDJFM) averages are used for consistency between data types. All PDO reconstruction indices were normalized to unit variance over 1901-2000; all other indices were normalized to unit variance overall, not just the reference period. The gray shading and black lines show the upper and lower 95% confidence limits of the PDO power spectrum derived from 140 realizations of a LIM simulation (eqn 3) each lasting 1750 years. d) Time series of each PDO reconstruction and the relative similarity of the reconstructions through time. The color lines show the individual reconstructions themselves (left axis), while the gray shading shows the relative similarity (right axis), measured by shared variance of the different indices through time, or the fraction of total variance shared by all reconstructions in the correlation matrix of all time series over a moving 40 year window. The ratio is computed by dividing the leading eigenvalue of the reconstruction correlation matrix by the total number of reconstructions available through time. e) Same time series as in (d) but smoothed with a 21-year running Gaussian filter.

Figure 12. Cold season relationship between climate indices discussed in this paper and US precipitation and temperature anomalies determined from climate division data (Vose

et al. 2014), for the years 1901-2014. (a-c) NDJFM US precipitation anomalies correlated with (a) the PDO index, (b) the ENSO index, and (c) the NPI. (d-f) NDJFM US temperature anomalies correlated with (d) the PDO index, (e) the ENSO index, and (f) the NPI.

Figure 13. NDJFM SST ENSO composites separated by high/low PDO values, determined over the years 1948-2008 from the ERSST v3b SST dataset. Shown are composites of the top quintile (El Nino) of the ENSO index segregated by (a) the top half and (b) the bottom half of the PDO indices for the 12 cases, and the bottom quintile (La Nina) of the ENSO index segregated by (a) the top half and (b) the bottom half of the PDO indices for the 12 cases. Each half of the quintile is determined by ranking the PDO values of the quintile years.

Figure 14. Summary figure of the basic processes involved in the PDO.

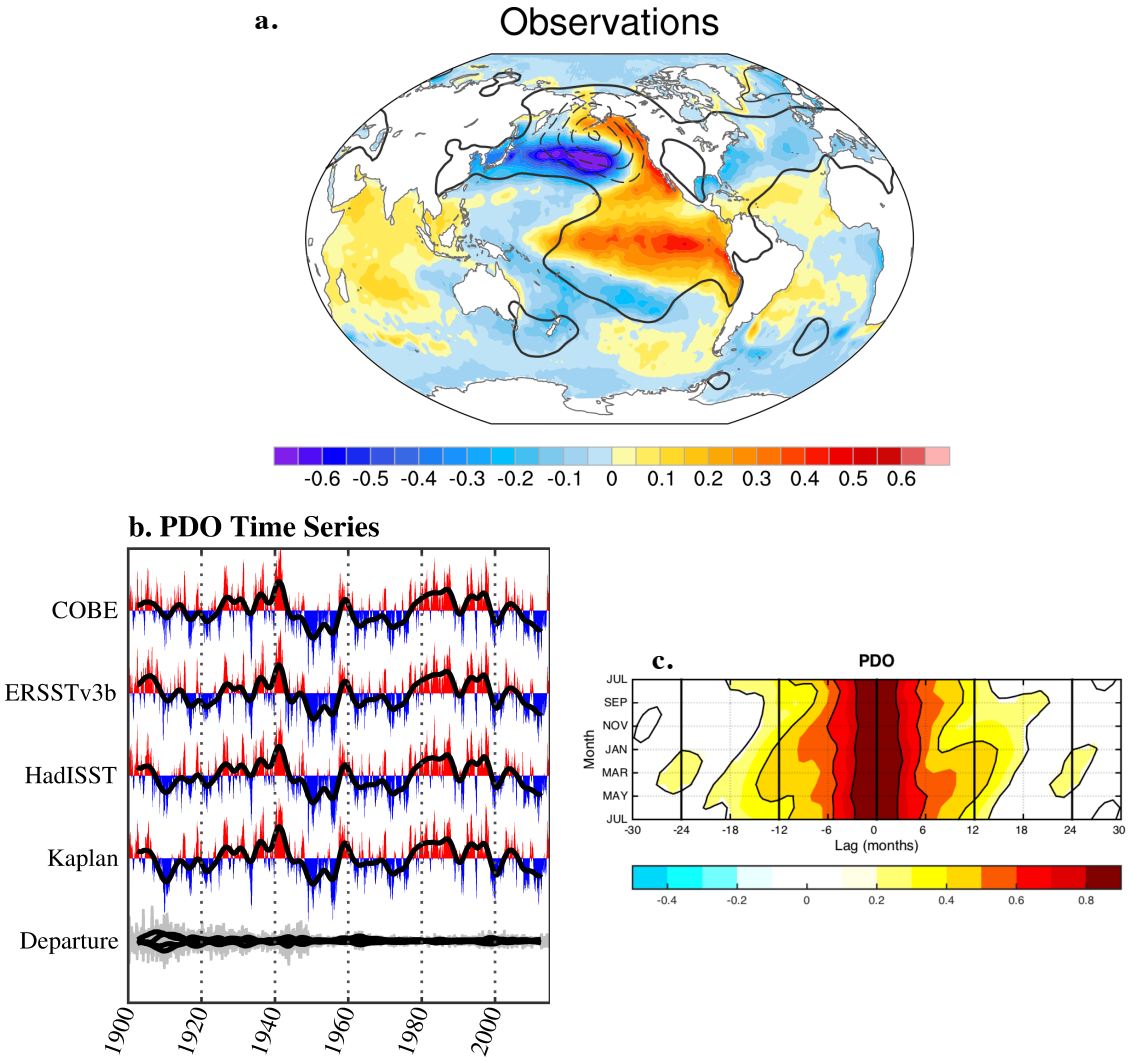

Figure 1. The Pacific decadal oscillation (PDO) over the historical record (1901-2014). (a) Regression of global monthly SST (shading) and DJF SLP (contours; interval is 1 hPa) anomalies onto the PDO time series from the HadISST dataset. Note that a *positive* PDO is associated with *negative* central North Pacific SSTA. (b) PDO index time series determined from the SST datasets, COBE (Ishii et al. 2005), ERSSTv3b (Smith et al. 2008), HadISST (Rayner et al. 200x), and Kaplan (Kaplan et al. 1998). The thick black line in each panel shows the smoothed (6-yr lowpass; Zhang et al. 1997) time series. The last panel shows the departure of each time series from the mean of all four time series. (c) Seasonal cycle of (3-month running mean) PDO index autocorrelation. Contour (shading) interval is 0.2 (0.1). Only values that are 95% significant are shaded. The month ordinate indicates the time of the PDO base month, and the lag indicates how far ahead/behind the PDO is; so, for example, the value plotted at (5, MAY) represents the correlation between the May value of the PDO and the subsequent October value of the PDO.

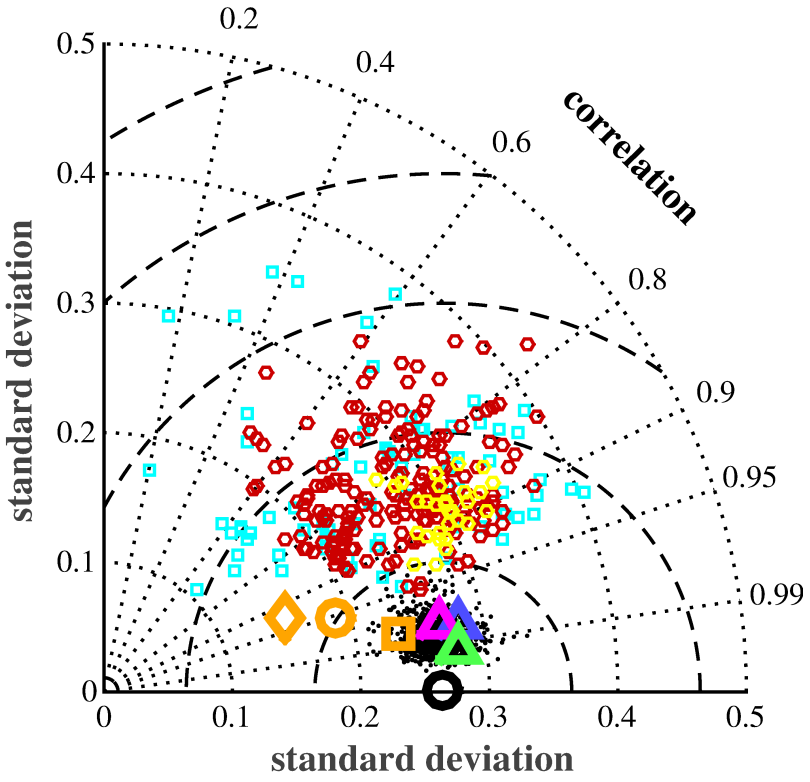

Figure 2. Taylor diagram (Taylor et al. 2001) comparing the reference PDO (HadISST) pattern (Fig. 1a, black circle) with variations due to sampling, observational dataset, and geographical domain; and to PDOs determined from CGCMs run with historical radiative forcing. In this diagram, the distance of a point from the origin is the pattern standard deviation normalized by the reference pattern standard deviation, and the distance from the reference point (at [1,0]) is the root mean square (rms) error normalized by the reference pattern standard deviation, indicated by the dashed semicircles spaced at an interval of 0.5. The pattern correlation, decreasing in a counterclockwise azimuthal direction, is mathematically related to these two quantities. The analysis is taken only over the North Pacific PDO domain (20°N-70°N). Black dots: PDO estimates based on the 50yr Monte Carlo subsamples; triangles: PDO determined from the ERSSTv3b (blue), COBE (green), and Kaplan (magenta) observed data sets; orange symbols: SSTA structure (within the North Pacific PDO region) associated with the leading SSTA EOF, where the southern border of the Pacific domain is instead 0º (square), 20ºS (diamond), and 70ºS (circle). Also shown are the CMIP3 (cyan), CMIP5 (red), and CESM-LE (yellow) historical simulation PDOs. EOF spatial patterns were interpolated to the 2° by 2° grid used for the reference pattern. Due to differences in landmasks, metrics for the Taylor diagram were calculated over ocean points that were in common between each model and the HadISST data.

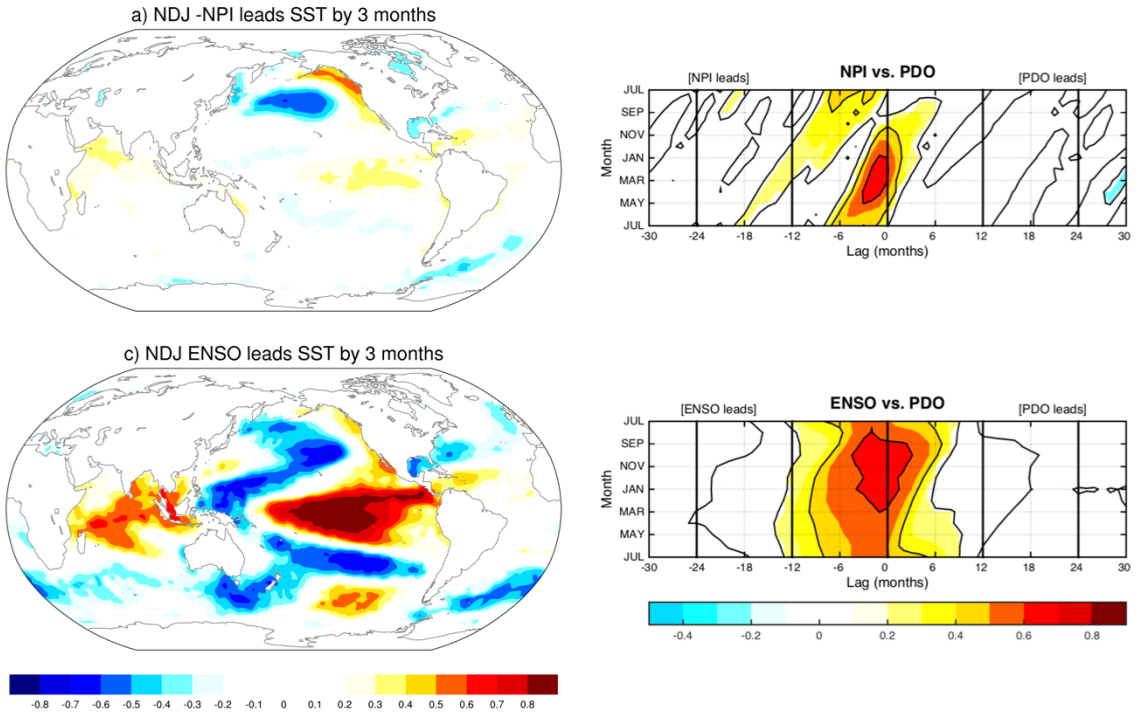

Figure 3. Illustration of how both local and remote atmospheric forcing can drive PDO variability. (a) One-season lead correlation between NDJ NPI and global SSTAs during FMA. (b) Seasonal cycle of cross correlation between the NPI and the PDO index (both filtered with 3-month running mean). PDO leads NPI for positive lags; NPI leads PDO for negative lags. In both panels (a) and (b), the NPI index sign has been flipped so that "positive" refers to a deepening of the Aleutian low, which also will correspond to positive PDO. (c) One-season lag correlation between the NDJ value of the "ENSO index" (the leading PC of tropical Pacific SSTA) and global SSTAs during FMA. (d) Seasonal cycle of cross correlation between the ENSO and PDO indices (both filtered with 3-month running mean). PDO leads ENSO for positive lags; ENSO leads PDO for negative lags. All figures are determined from 1901-2014 data; shading interval is 0.1. For panels (b) and (d), only values that are 95% significant are shaded, and the contour line interval is 0.2. The month ordinate indicates the time of the PDO index base month, and the lag indicates how far ahead/behind the second variable is; so, for example, the value plotted at (5, MAY) represents the correlation between the May value of the PDO and the subsequent October value of the other variable.

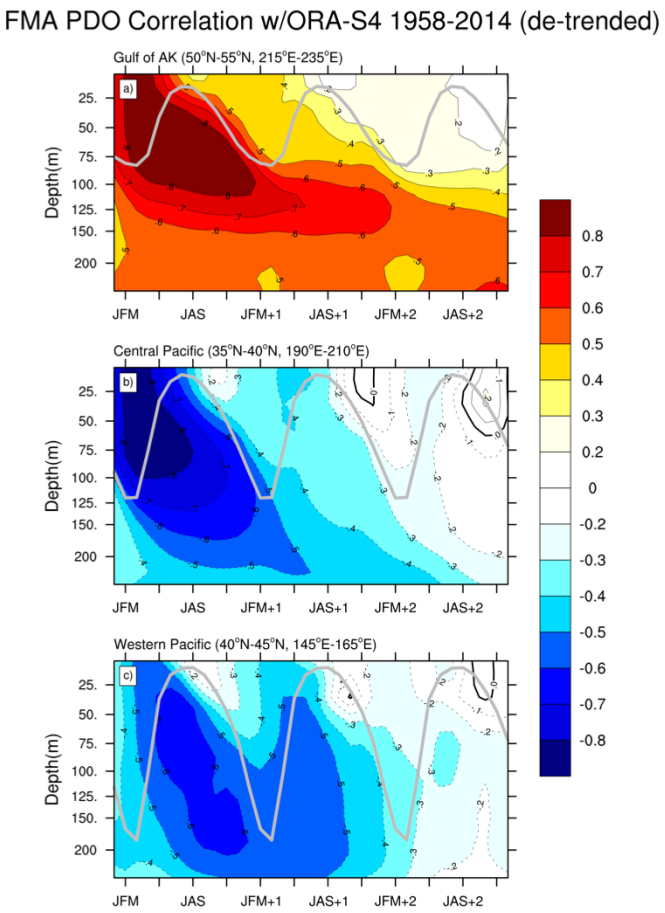

Figure 4. Illustration of re-emergence of oceanic thermal anomalies. Correlation of the JFM value of the PDO index (as in Fig. 1b except determined from 3-month running means) with ECMWF ORAS4 ocean temperatures (Balmaseda et al. 2013) for the subsequent two years, area averaged in (a) the Gulf of Alaska, (b) the central Pacific, and (c) the west Pacific, for the years 1958-2014. The gray line shows the climatological mean mixed layer depth as a function of time of year at each location, so it repeats over the three year period.

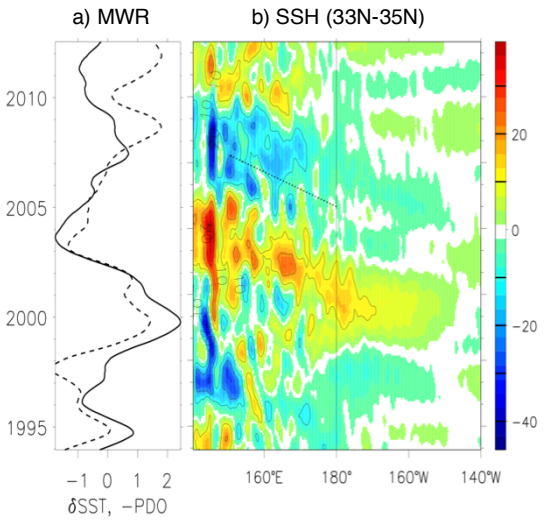

Figure 5. Illustration of the slow ocean (Rossby wave) dynamics process driving PDO variability. (a) Time series of the SSTA in the mixed water region (MWR, solid) and the PDO index (dashed, with sign inverted). The temperature index is based on the optimal interpolation, blended, quarter degree SST analysis of Reynolds et al. (2007). The MWR extends from the coast of Japan to 150E, and between 36N to 42N. Both the MWR and PDO indices have been normalized by their respective standard deviation. The correlation between MWR and PDO indices is -0.49. (b) Satellite observed sea surface height anomalies in cm, averaged between 33N and 35N. The dotted line marks a westward phase speed of 3.7 cm/s (Qiu and Chen 2010). Sea surface temperature and sea surface height anomalies have been detrended and smoothed with a two year running mean, with weights varying linearly as a function of lag.

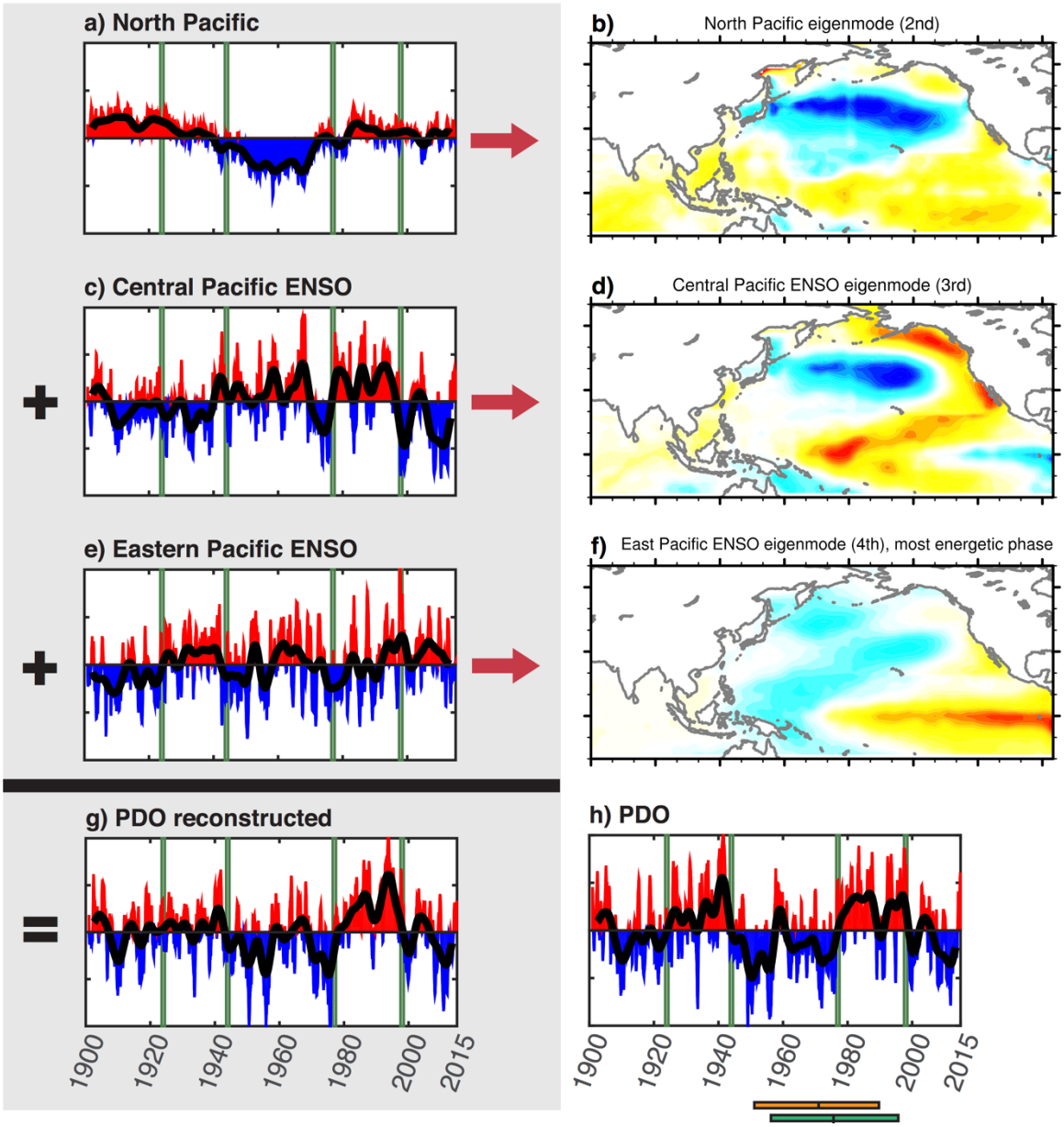

Figure 6. Reconstructing the PDO as the sum of three different dynamical processes. (a-h) Contributions to the PDO from (a) the second ("North Pacific"; Fig. 6b), (c) third ("Central Pacific ENSO"; Fig. 6d) and (e) fourth ("Eastern Pacific ENSO"; Fig. 6f shows most energetic phase of this complex eigenmode [essentially, cosine phase], with least energetic phase [sine phase] not shown) eigenmodes of the LIM described in the paper. Note that unlike EOFs, these eigenmodes are nonorthogonal. Contour interval is the same in all three eigenmode panels; all eigenmodes are normalized to have unit amplitude. The LIM is determined in a reduced EOF space (with 25 degrees of freedom) that retains about 85% of the SST variance in the Tropics and North Pacific domains. (d) "PDO reconstruction", the sum of the time series shown in panels a, c, and e. (h) PDO index time series (same as Fig. 1c but with three-month running mean smoothing applied). In the time series panels, heavy black lines represent the application of the same 6-yr lowpass smoother as in Fig. 1b, and vertical green lines indicate times of PDO "regime shifts".

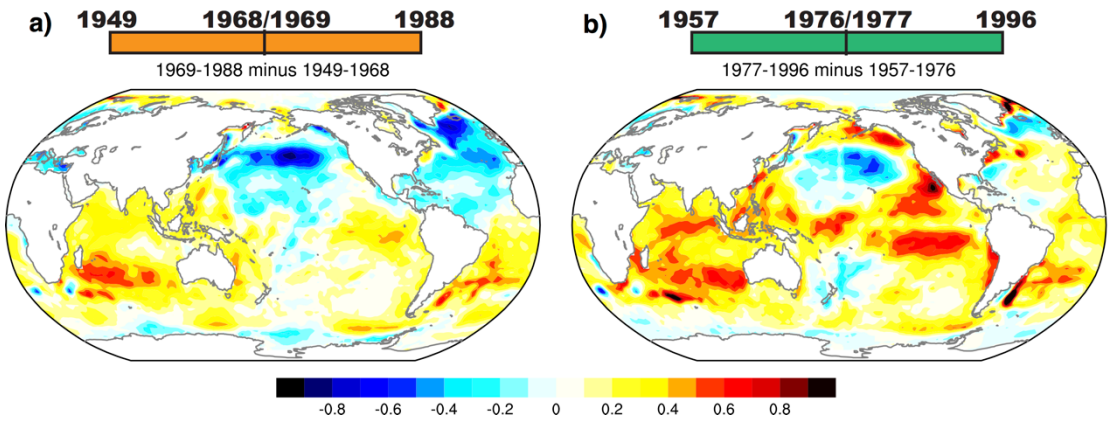

Figure 7. Epoch difference maps, showing SST differences between two adjacent 20 year means centered on (a) 1968/69 and (b) 1976/77. The adjacent 20-year periods used for each epoch calculation are indicated by the corresponding color bars in Fig. 6h.

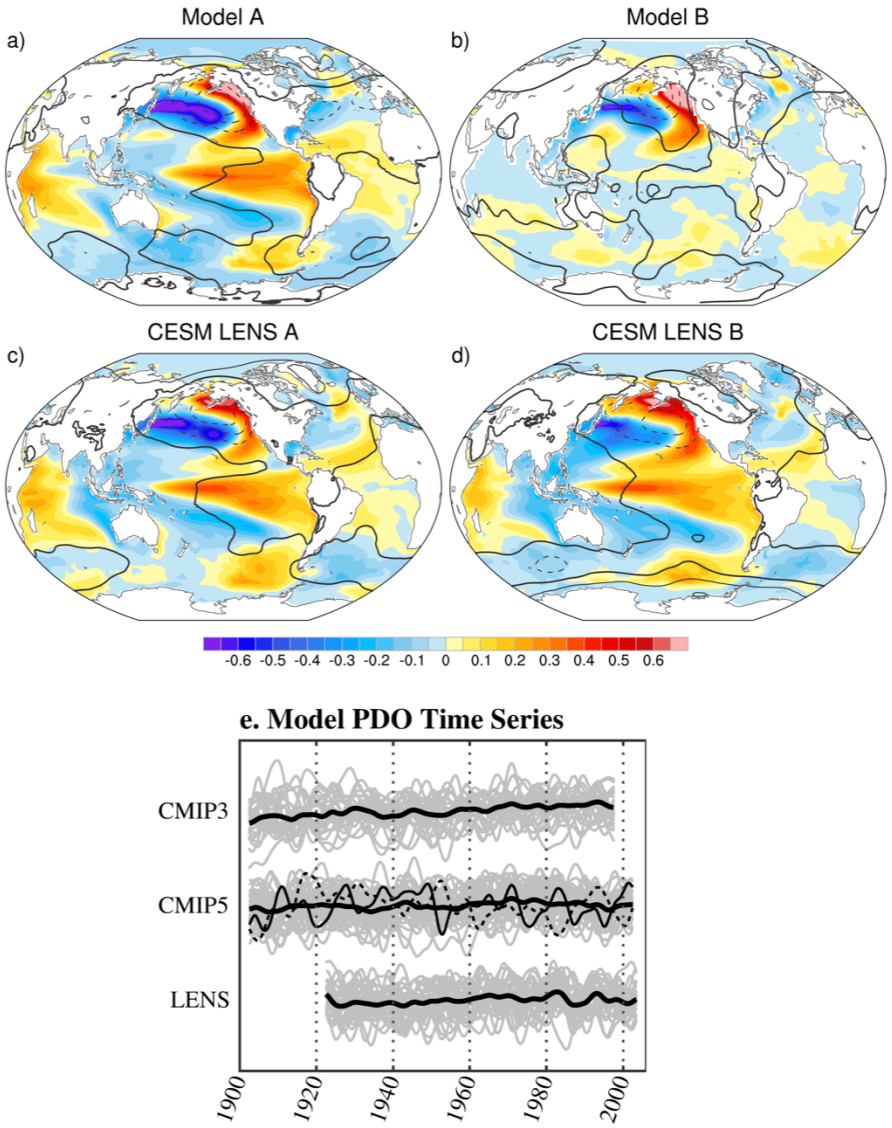

Figure 8. The PDO over the historical record as simulated by coupled CGCMs. (a and b) Same as Fig. 1a except showing two selected members of the "historical" CMIP5 ensemble that are (a) closest and (b) farthest from the reference pattern in Fig. 2. (c and d) Same as Fig. 8a except showing two selected members of the CESM-LE that are (c) closest and (d) farthest from the reference pattern in Fig. 2. (e) PDO time series from all ensemble members; all time series are smoothed with the Zhang et al. filter (used in Fig. 1c). Thin gray lines represent each ensemble member, the thin black solid (dashed) line in the CMIP5 panel represents model A (B), and the thick black line is the ensemble mean for each set of models.

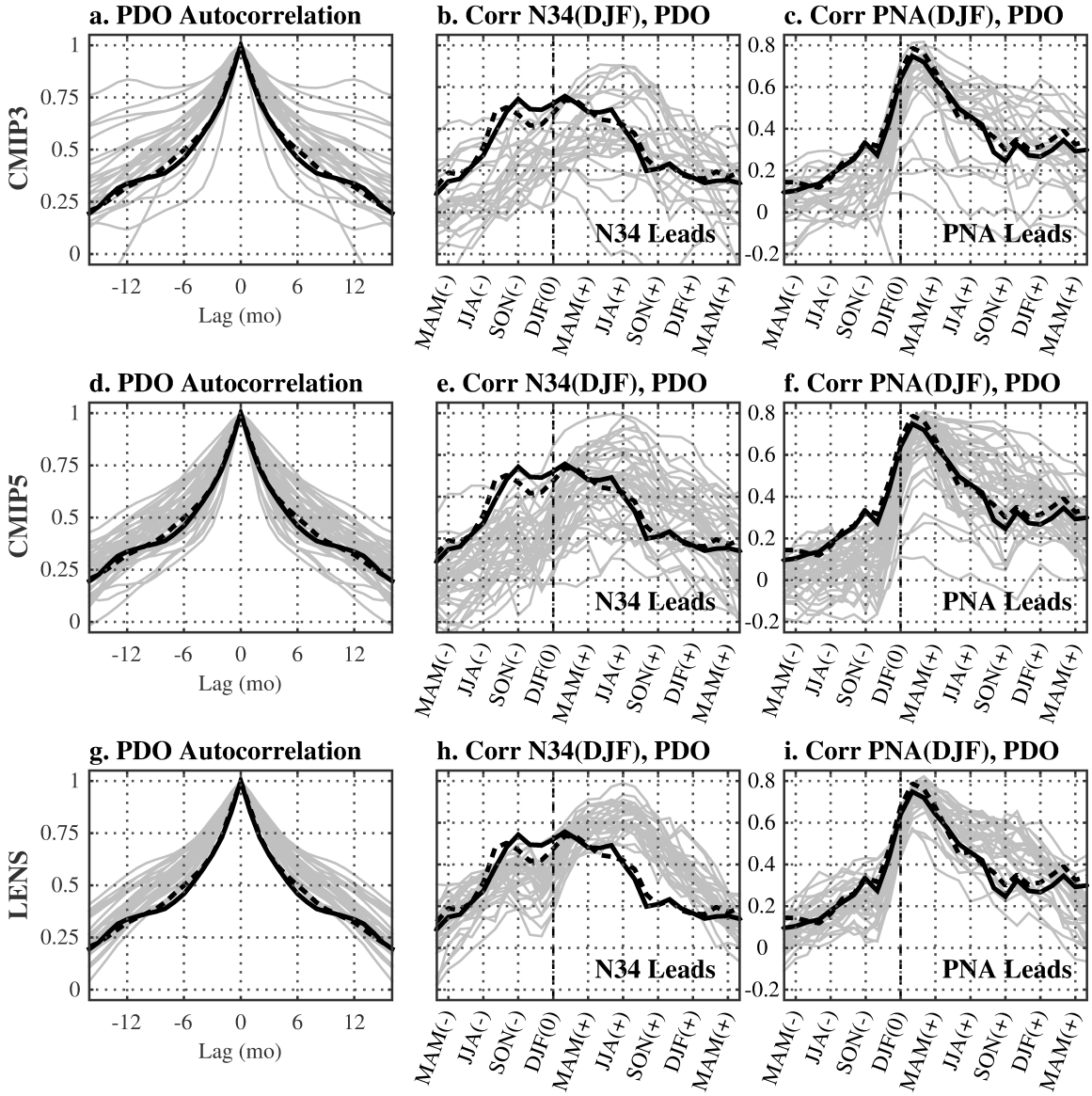

Figure 9. Temporal relationships relevant to the PDO for the CMIP3 (top row), CMIP5 (middle row), and LENS (bottom row) ensembles. Shown are: (a, d, g) the autocorrelation of the monthly PDO index; (b, e, h) the lagged seasonal correlation between the seasonal PDO index and the DJF averaged Nino 3.4 index; and (c, f, i) the lagged seasonal correlation between the seasonal PDO index and the DJF averaged PNA index. On all plots thin grey lines indicate model correlations, the thick solid black line indicates correlations for indices from the HadISST data, and the thick dashed line indicates correlations with indices from the ERSSTv3b data. For panels (c, f, i) the observed DJF PNA time series is obtained from the 20th Century Reanalysis. Observed correlations are taken over the time period 1901-2009, CMIP3 over 1900-1999, CMIP5 over 1901-2004, and LENS over 1920-2005. For seasonal correlations, positive lags indicate that the Nino 3.4 or PNA index leads the seasonal PDO index, and the label on the abscissa indicates the season for which the PDO is defined.

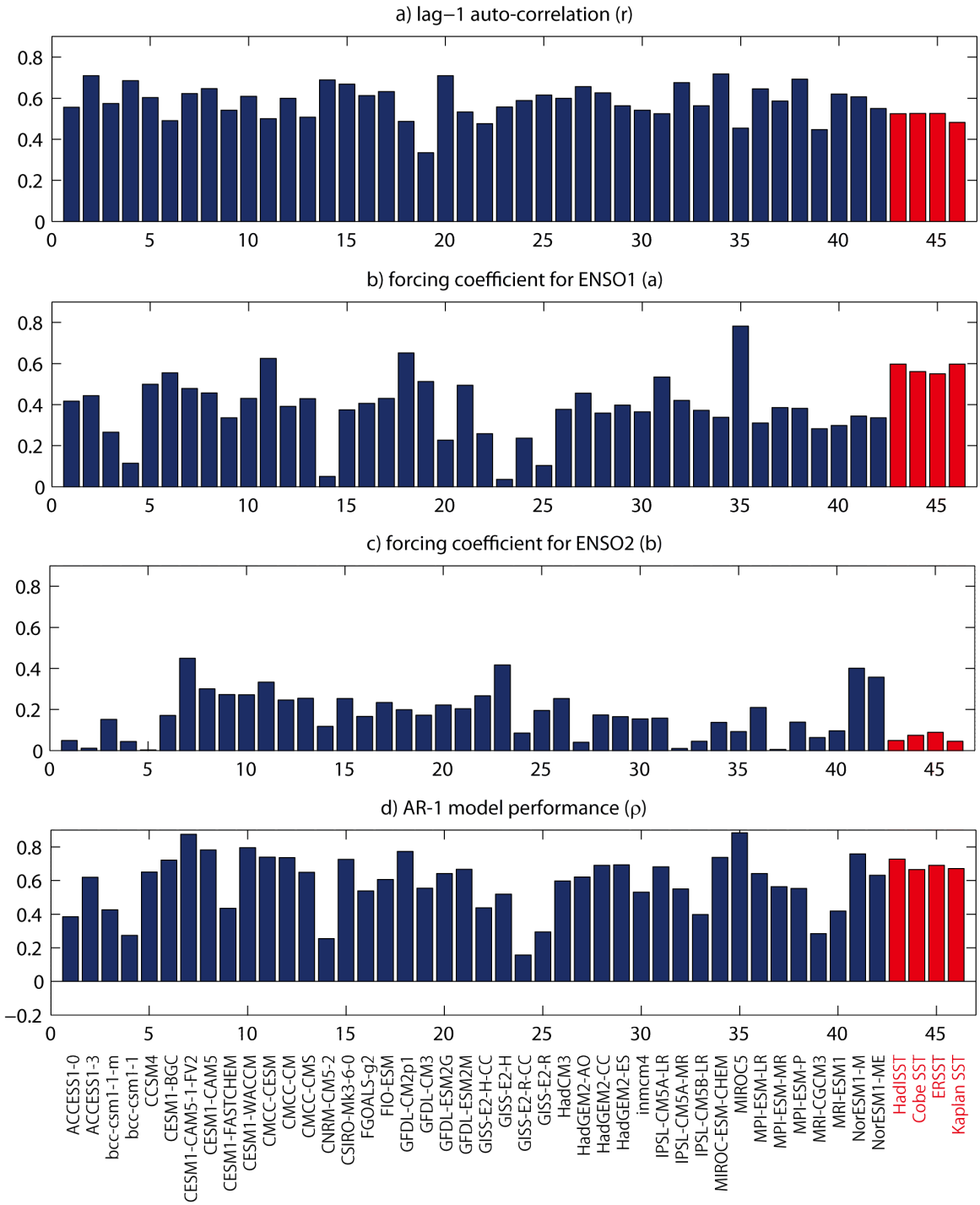

Figure 10. Parameters for an AR-1 model of the PDO time series, PDO(n)=*r* PDO(n-1) + *a* ENSO1(n) + *b* ENSO2(n) + ε, for CMIP5 models (blue bars) and observations (red bars). The AR-1 model is determined from the PDO index and two leading tropical PCs, ENSO1 and ENSO2, calculated as discussed in the text but for the period 1900 to 2000, and then averaged from July to June. (a) Unforced lag-1 auto correlation, i.e., *r* in the above equation. (b) Forcing coefficient for ENSO1, i.e., *a* in the above equation. (c) Forcing coefficient for ENSO2, i.e., *b* in the above equation. (d) Correlation ρ between each model's PDO index time series and the corresponding estimated PDO timeseries determined from the AR-1 model.

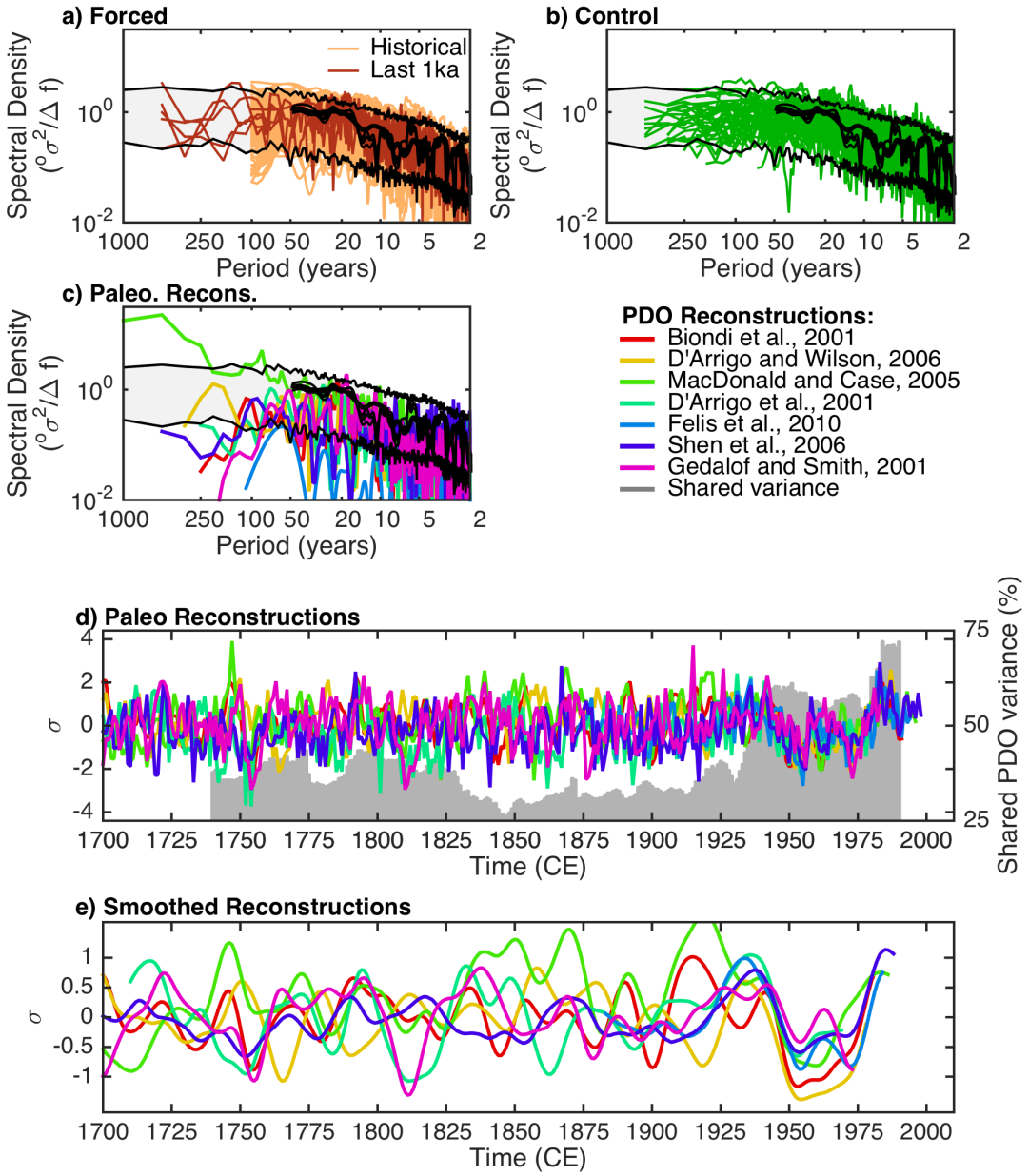

Figure 11. Comparison of observed, paleoclimate, and CMIP5 PDO spectra: (a) CMIP5 "historical" simulations (190 runs total) and forced "last millennium" (past 1000 yrs) simulations (6 runs); (b) unforced "control" simulations (48 runs total); and (c) paleoclimate (tree ring and other proxy-based) reconstructions of the PDO. In panels (a-c), the thick black line represents the HadISST PDO spectrum, and the three thin blacks lines the other three observational PDO spectra. In each case, only winter (NDJFM) averages are used for consistency between data types. All PDO reconstruction indices were normalized to unit variance over 1901-2000; all other indices were normalized to unit variance overall, not just the reference period. The gray shading and black lines show the upper and lower 95% confidence limits of the PDO power spectrum derived from 140 realizations of a LIM simulation (eqn 3) each lasting 1750 years. d) Time series of each PDO reconstruction and the relative similarity of the reconstructions through time. The color lines show the individual reconstructions themselves (left axis), while the gray shading shows the relative similarity (right axis), measured by shared variance of the different indices through time, or the fraction of total variance shared by all reconstructions in the correlation matrix of all time series over a moving 40 year window. The ratio is computed by dividing the leading eigenvalue of the reconstruction correlation matrix by the total number of reconstructions available through time. e) Same time series as in (d) but smoothed with a 21-year running Gaussian filter.

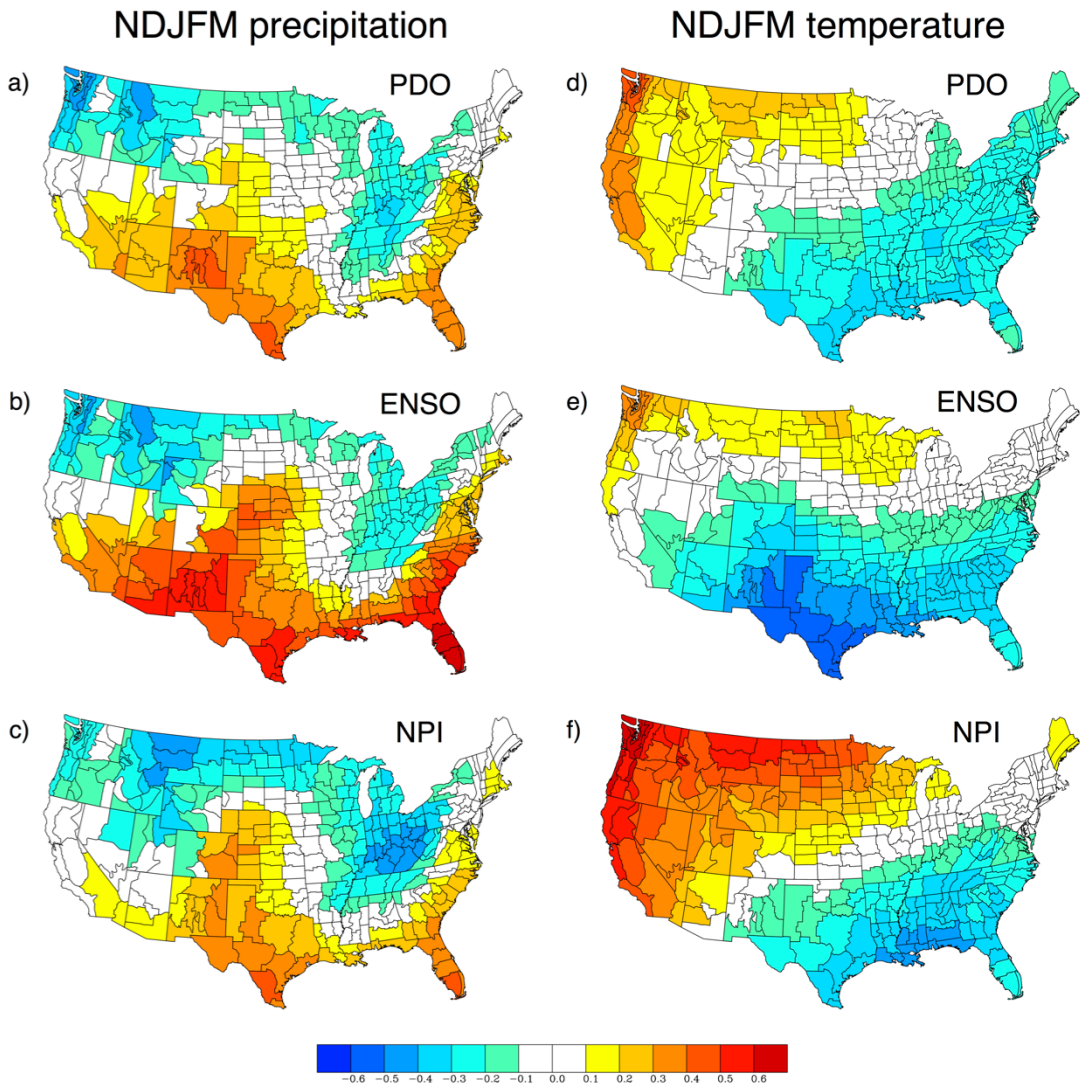

Figure 12. Cold season relationship between climate indices discussed in this paper and US precipitation and temperature anomalies determined from climate division data (Vose et al. 2014), for the years 1901-2014. (a-c) NDJFM US precipitation anomalies correlated with (a) the PDO index, (b) the ENSO index, and (c) the NPI. (d-f) NDJFM US temperature anomalies correlated with (d) the PDO index, (e) the ENSO index, and (f) the NPI.

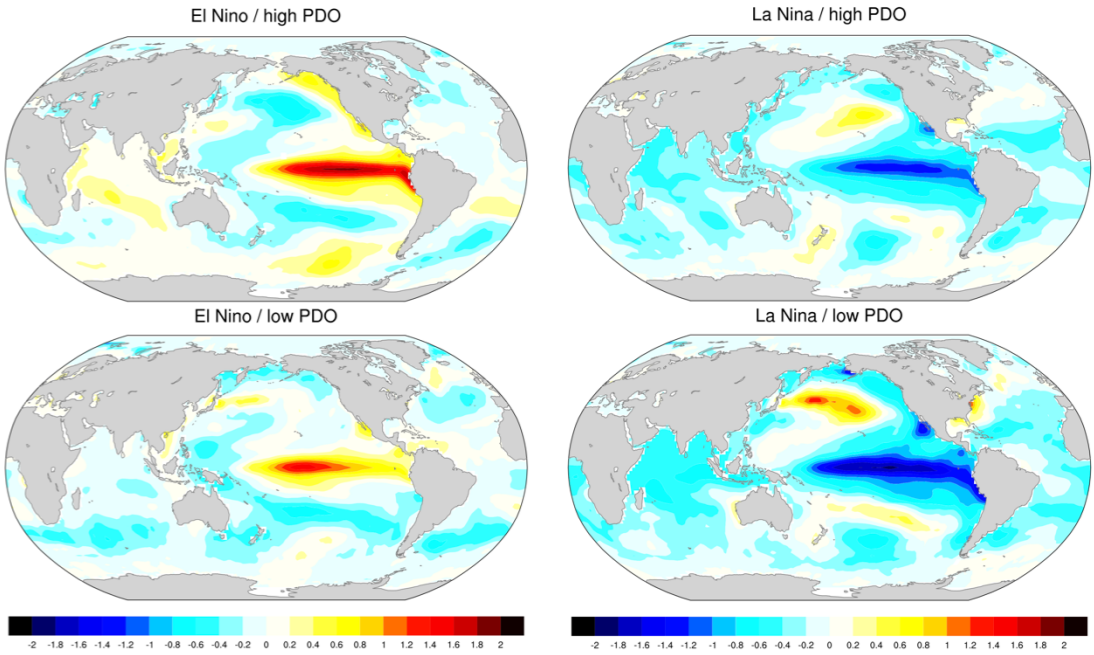

Figure 13. NDJFM SST ENSO composites separated by high/low PDO values, determined over the years 1948-2008 from the ERSST v3b SST dataset. Shown are composites of the top quintile (El Nino) of the ENSO index segregated by (a) the top half and (b) the bottom half of the PDO indices for the 12 cases, and the bottom quintile (La Nina) of the ENSO index segregated by (a) the top half and (b) the bottom half of the PDO indices for the 12 cases. Each half of the quintile is determined by ranking the PDO values of the quintile years.

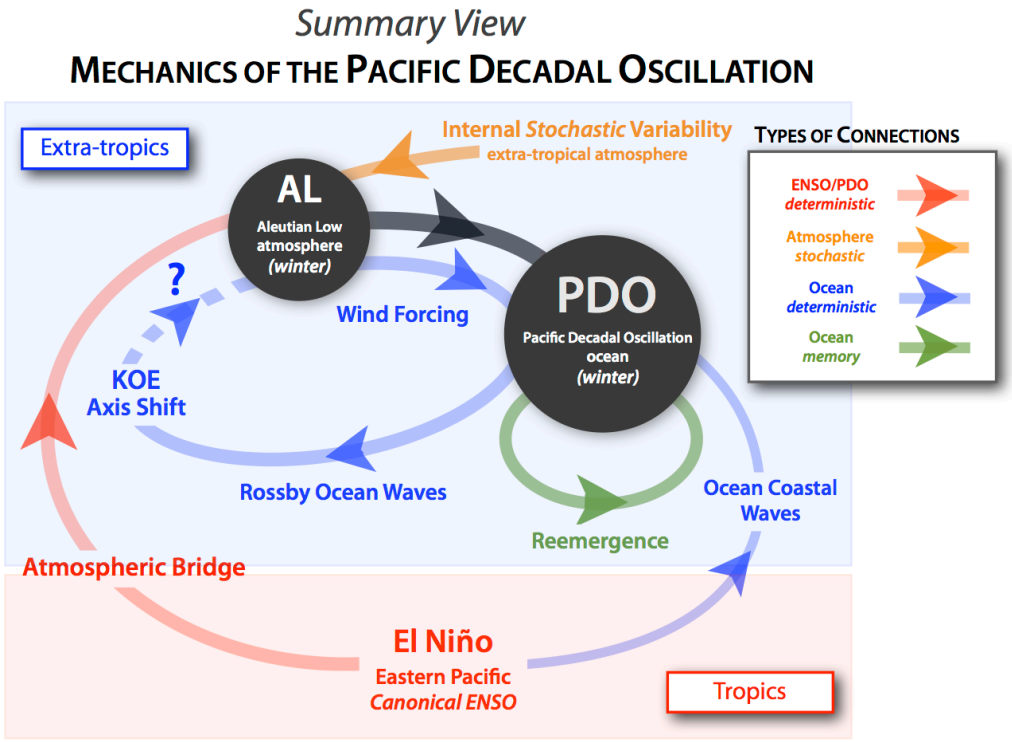

Figure 14. Summary figure of the basic processes involved in the PDO.